Application of Novel Hybrid Mesh Generation Methodologies for Improved Unstructured CFD Simulations
AIAA 2010-4672

Simone Crippa

DLR Institute of Aerodynamics and Flow Technology Braunschweig

$C^2A^2S^2E$ Branch

DLR Deutsches Zentrum für Luft- und Raumfahrt e.V.
in der Helmholtz-Gemeinschaft

Overview

- Introduction & Cases
- Computational Methods
- Initial Results
- Up-Front Grid Improvements
- Grid Family
- Adjoint-based Grid Improvements
- Workshop Summary
- Post-Workshop Activities
- Conclusions

Introduction

- NASA common research model; cruise configuration of conventional civil transport aircraft
- WBT-configuration selected as experimental basis for the fourth Drag Prediction Workshop (DPW4)
- “Natural application” of Solar grid generation package due to available philosophy files, which automate the definition of sources

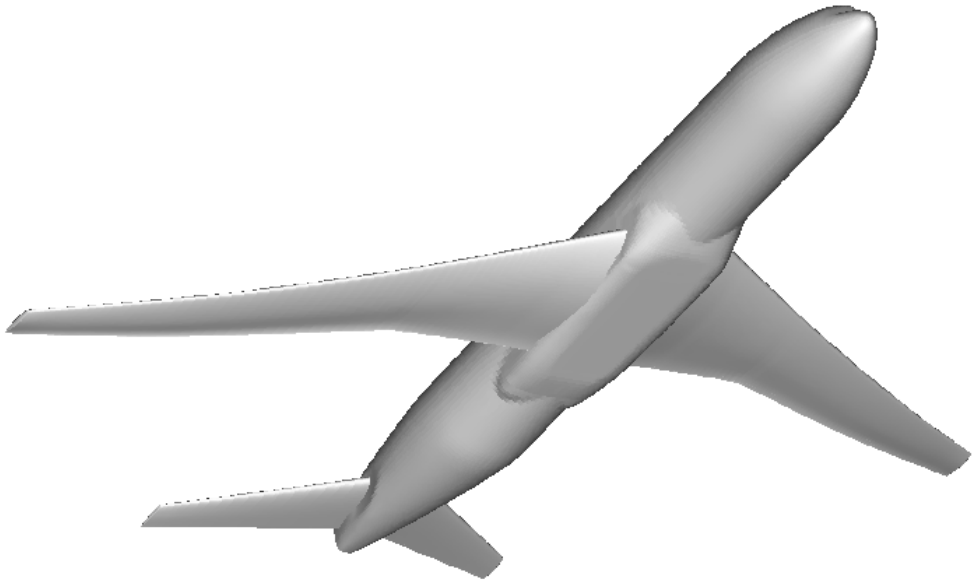

Cases

- Workshop held in San Antonio, TX, on June 20-21 2009
- **case 1** – consisting of two sub-cases
  - **1)** grid convergence study at M = 0.85, C-lift = 0.5, Re = $5 \cdot 10^6$
    - tail incidence angle iH = 0°
    - coarse, **medium** and fine grids
  - **2)** downwash study at M = 0.85
    - drag polars for alpha = 0.0°, 1.0°, 1.5°, 2.0°, 2.5°, 3.0°, **4.0°**
    - tail incidence angles iH = -2°, **0°**, +2°, and tail off
    - medium grid
    - trimmed drag polar derived from polars at iH = -2°, 0°, +2°
    - delta drag polar of tail-off vs. tail-on
  - three turbulence models (SAO, SST, RSM)
- case 3 – Reynolds number effects (WT to flight scaling)
  - Same configuration & settings as case 1.1, but with Re = $20 \cdot 10^6$

Computational Methods

- DLR **TAU** code (CFD) and ARA/BAE-ATC **Solar** (grid gen.)

- Compressible RANS
- Unstructured, finite volume, node-centered, (Full-NS)
- Central scheme with Jameson-type scalar dissipation; k_2=1/4 k_4=1/64
- Backward-Euler, LUSGS
- 4w multigrid / sg
- SA(RC), Menter k-ω SST, SSG/LLR-ω RSM

- Unstructured, quad/hexa-dominant
- Advancing-layer/front
- Octree-based background grid for steering Delaunay tetra generation
- Anisotropic surface quads
- Adaptive, variable expansion ratio
- No user-specified amount of wall-normal layers

Initial Results

- Initial medium grid (~10 mio. Points) generated in ½ day, using default philosophy files

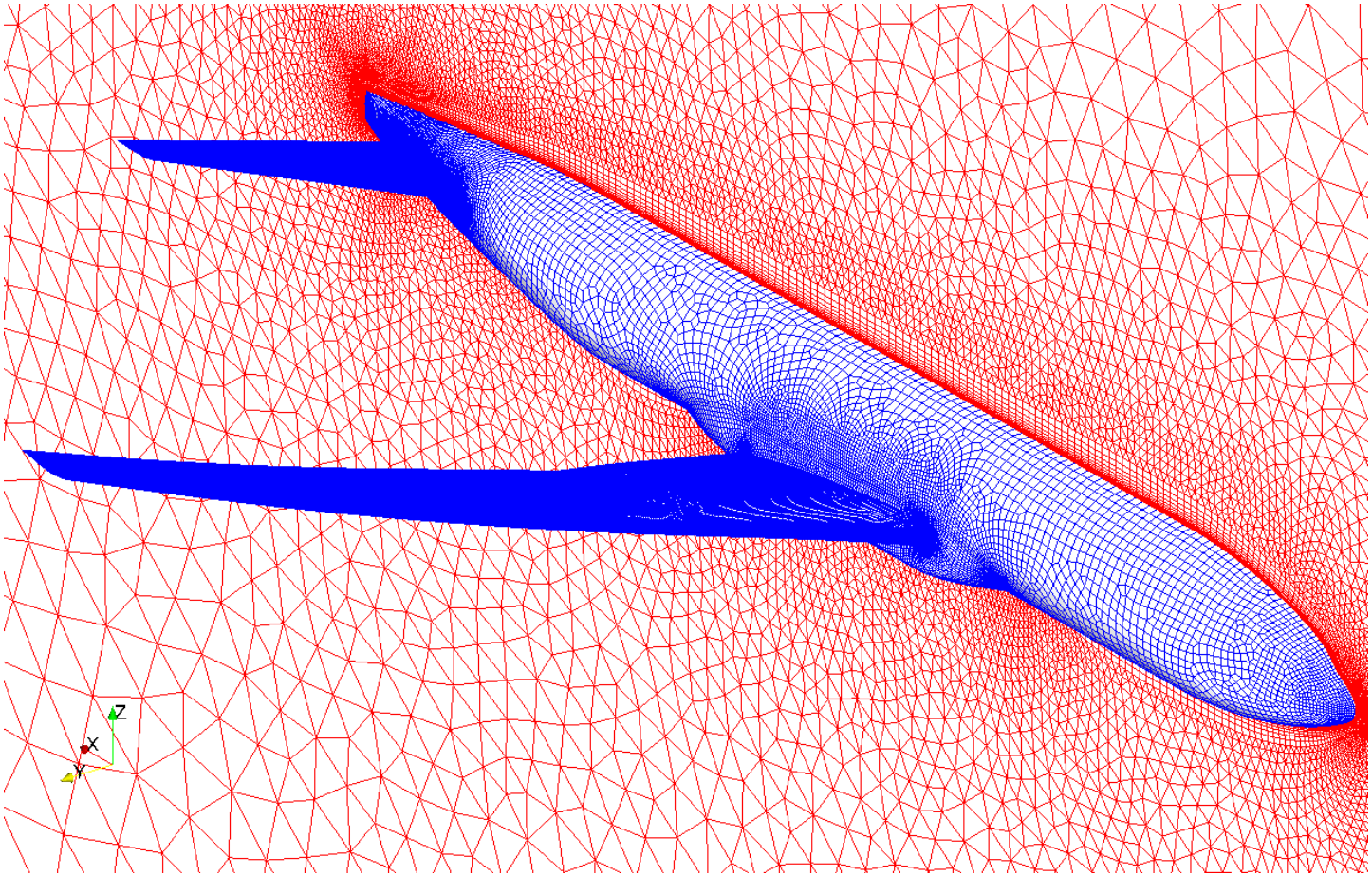

Initial Results

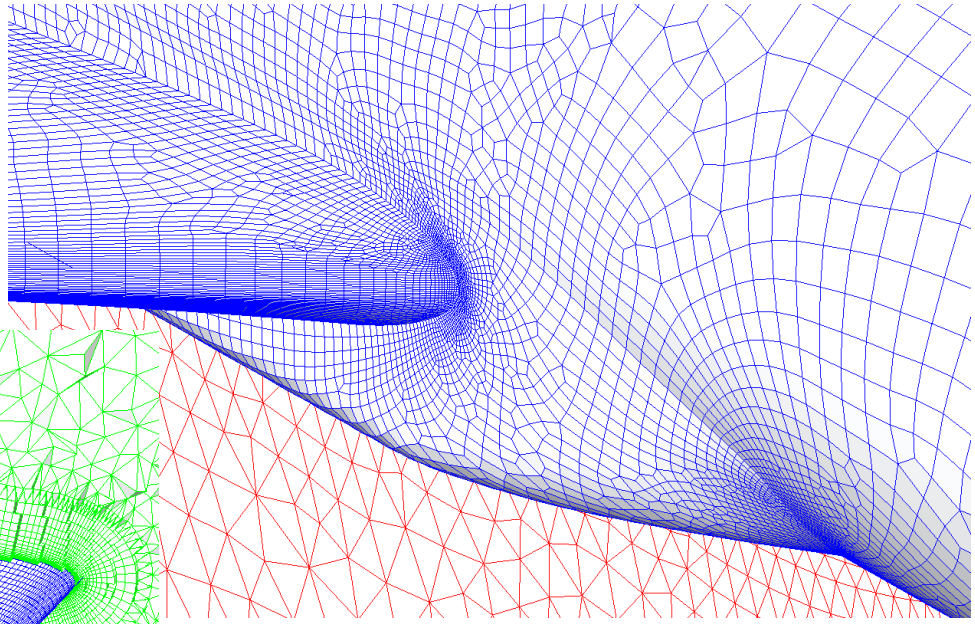

Wing-fuselage fairing

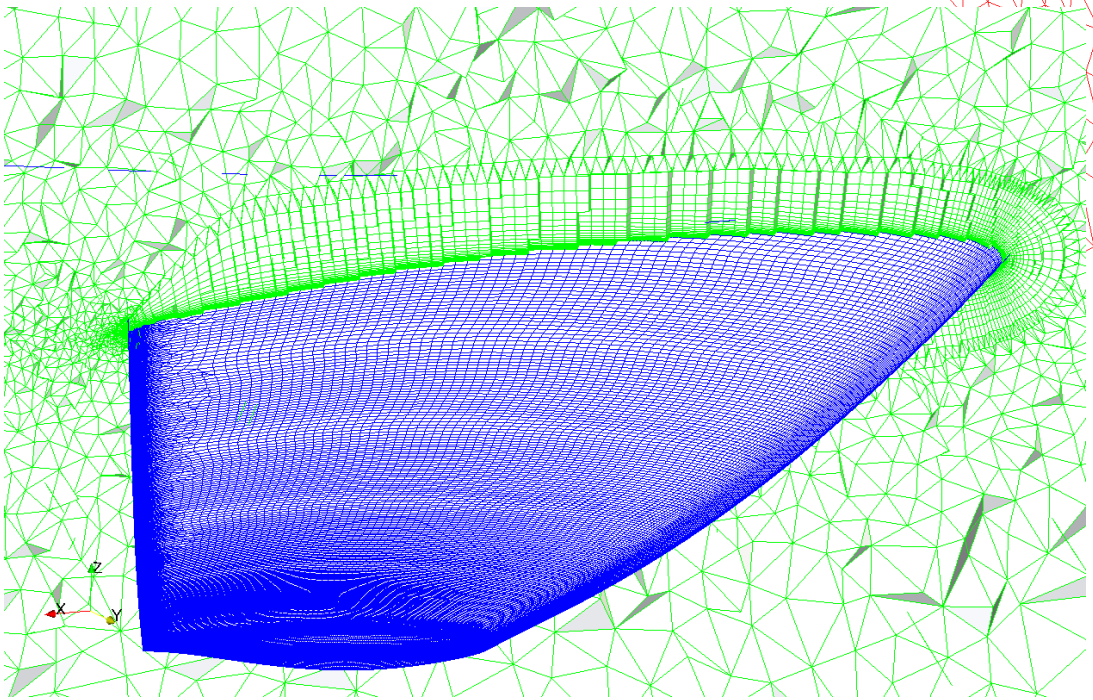

Field-cut around outboard wing

Initial Results

- Overnight initial results; acceptable solver convergence

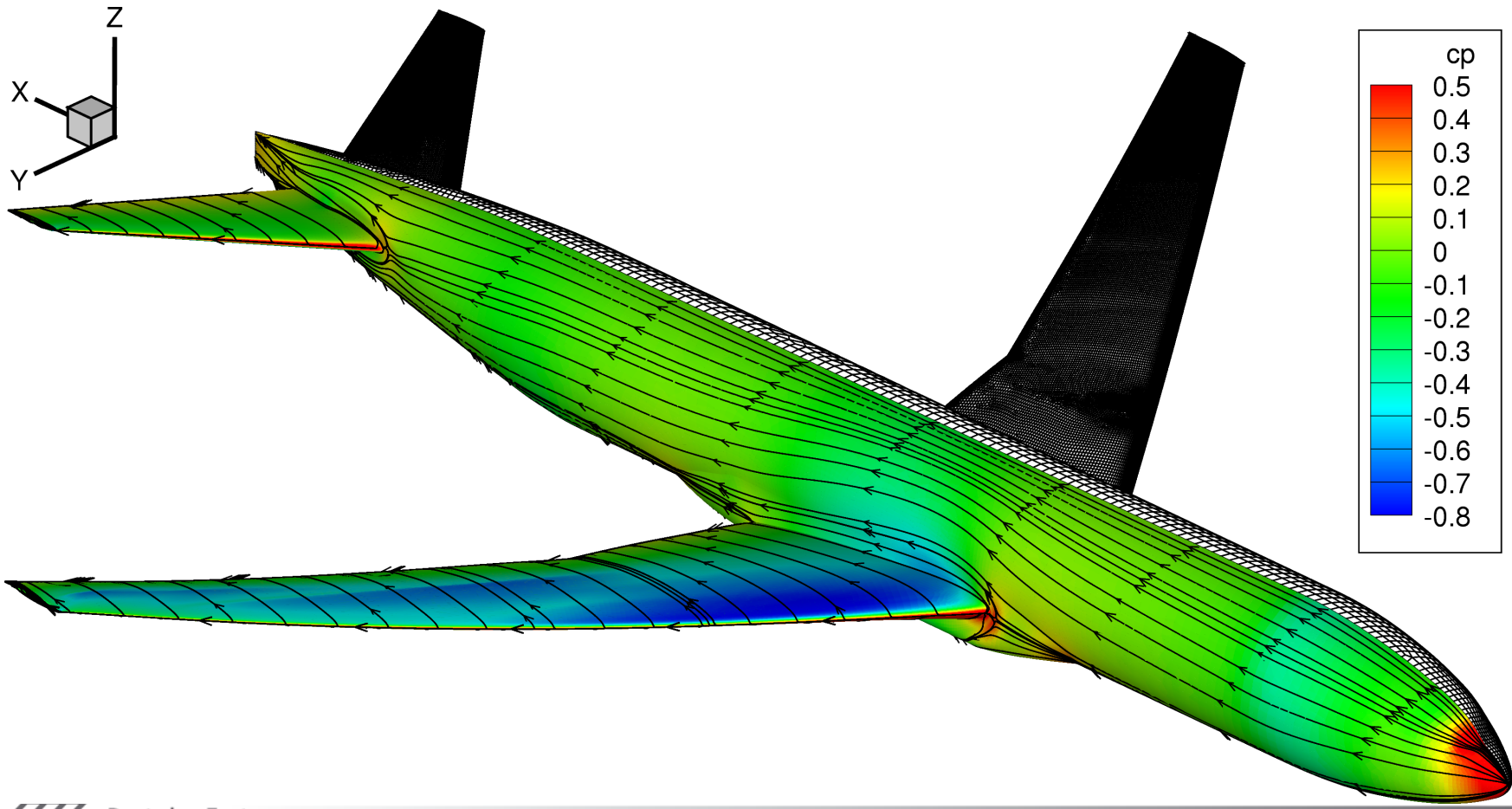

Up-Front Grid Improvements

- Strict application of DPW committee gridding guidelines leads to contracted near-field layer at concave corners

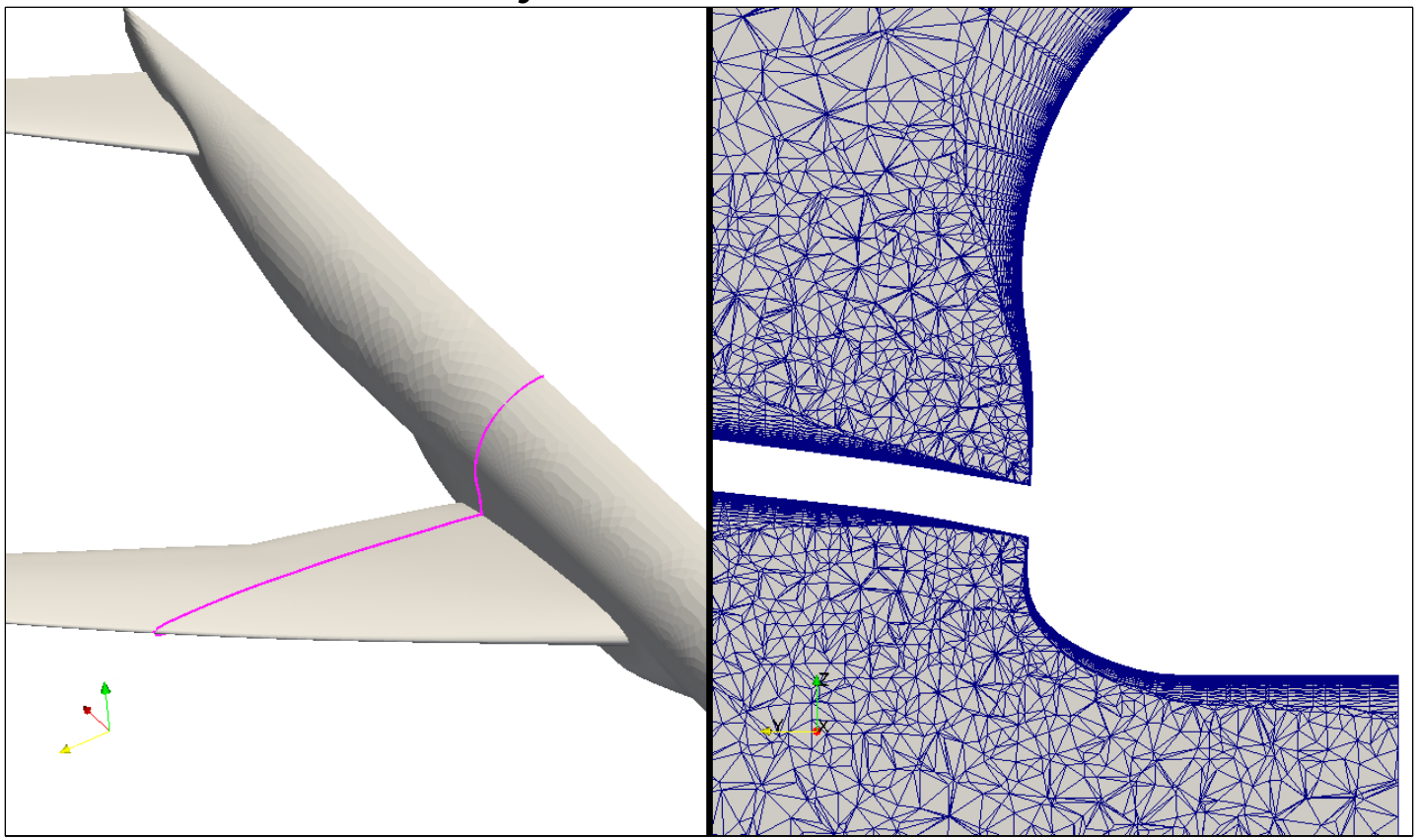

Cut at x=1400”

Up-Front Grid Improvements

- Increase of surface grid size at junctions mitigates, but does not resolve the problem

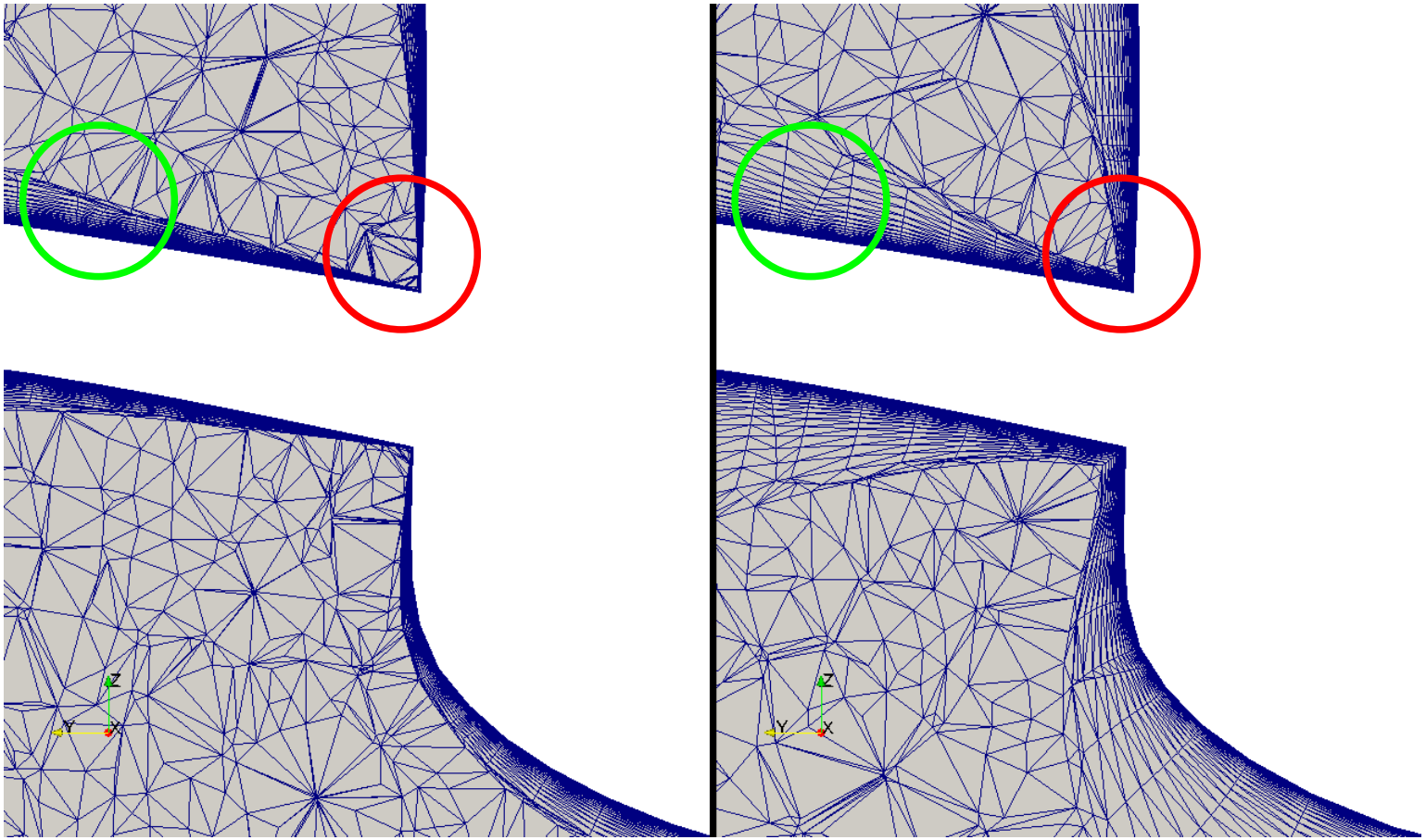

Up-Front Grid Improvements

- After initial runs with medium grid, additional anisotropic source added at mid-chord, over entire span, to better resolve shock region

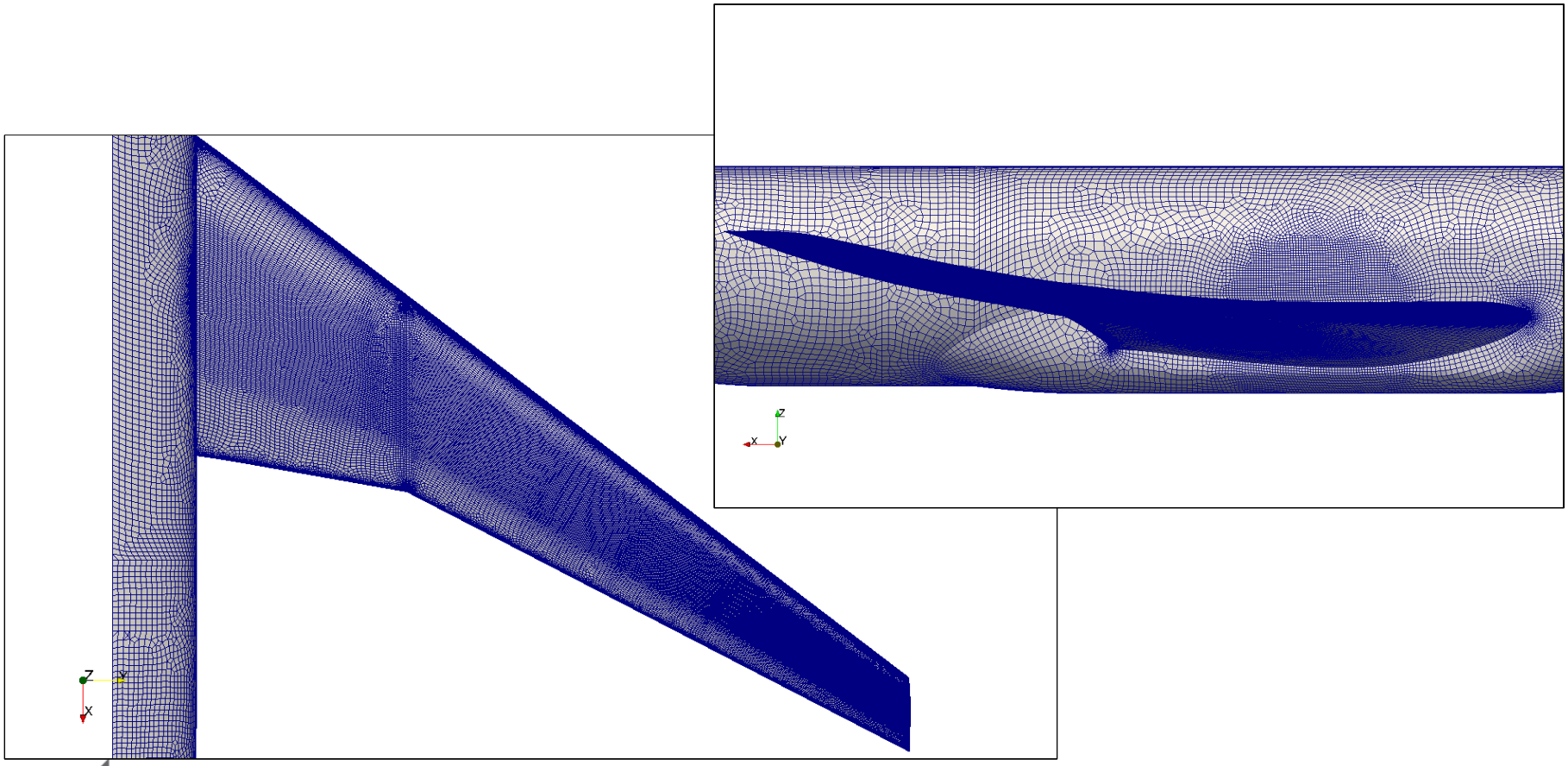

Up-Front Grid Improvements

- Modification of fuselage trailing edge
  - Sharp → blunt; through cut at x=2561.5 inch (bTE: 0.5 inch)

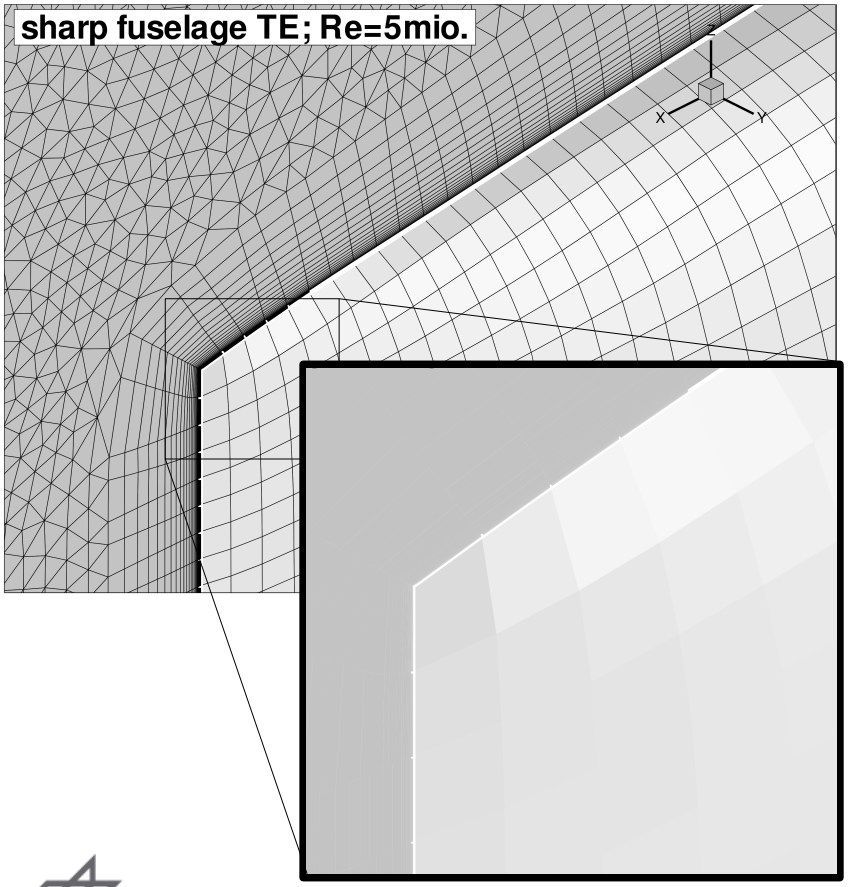

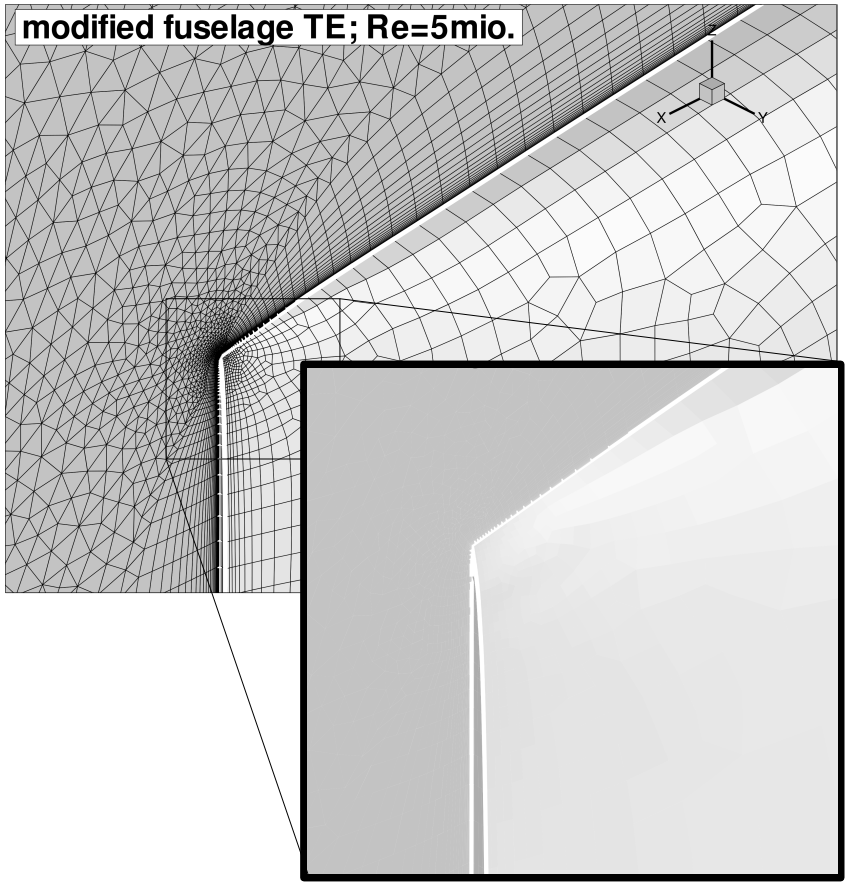

Grid Family

- Starting from medium source distribution, generation of one level of finer and coarser grids
  - Source sizes scaled by a factor of $\sqrt[3]{3}$ (≈ 1.4422), affecting both surface and volume meshing
  - Influence radii (r_1 & r_2) not changed, being coupled to geometry
  - Consistent scaling of expansion ratio, to keep the total near-field layer extent similar between grid levels

$$Total\ layer\ thickness = \sum_{i=0}^{n} a \cdot q^i = a \cdot \frac{1-q^{n+1}}{1-q}$$

a: first layer spacing
q: expansion ratio
N: Number of layers (n+1)

Grid level 2 being finer than grid level1: $a_2 = a_1 / \sqrt[3]{3}$, $N_2 = N_1 \cdot \sqrt[3]{3}$

$$a_1 \cdot \frac{1-q_1^{N_1}}{1-q_1} = a_2 \cdot \frac{1-q_2^{N_2}}{1-q_2}$$

Grid Family

- Final grid family

Grid	Coarse	Medium	Fine
# cells on blunt TE	8	12	18
Surface point	$130 \cdot 10^3$	$271 \cdot 10^3$	$566 \cdot 10^3$
Max. # of wall-normal layers	30	42	60
Expansion ratio	1.3009	1.2	1.135
# points in nearfield	$3.47 \cdot 10^6$	$9.94 \cdot 10^6$	$28.69 \cdot 10^6$
# of tetra cells	$5.31 \cdot 10^6$	$14.31 \cdot 10^6$	$38.58 \cdot 10^6$
Total # of points	**$4.07 \cdot 10^6$**	**$11.70 \cdot 10^6$**	**$34.08 \cdot 10^6$**

Grid Family

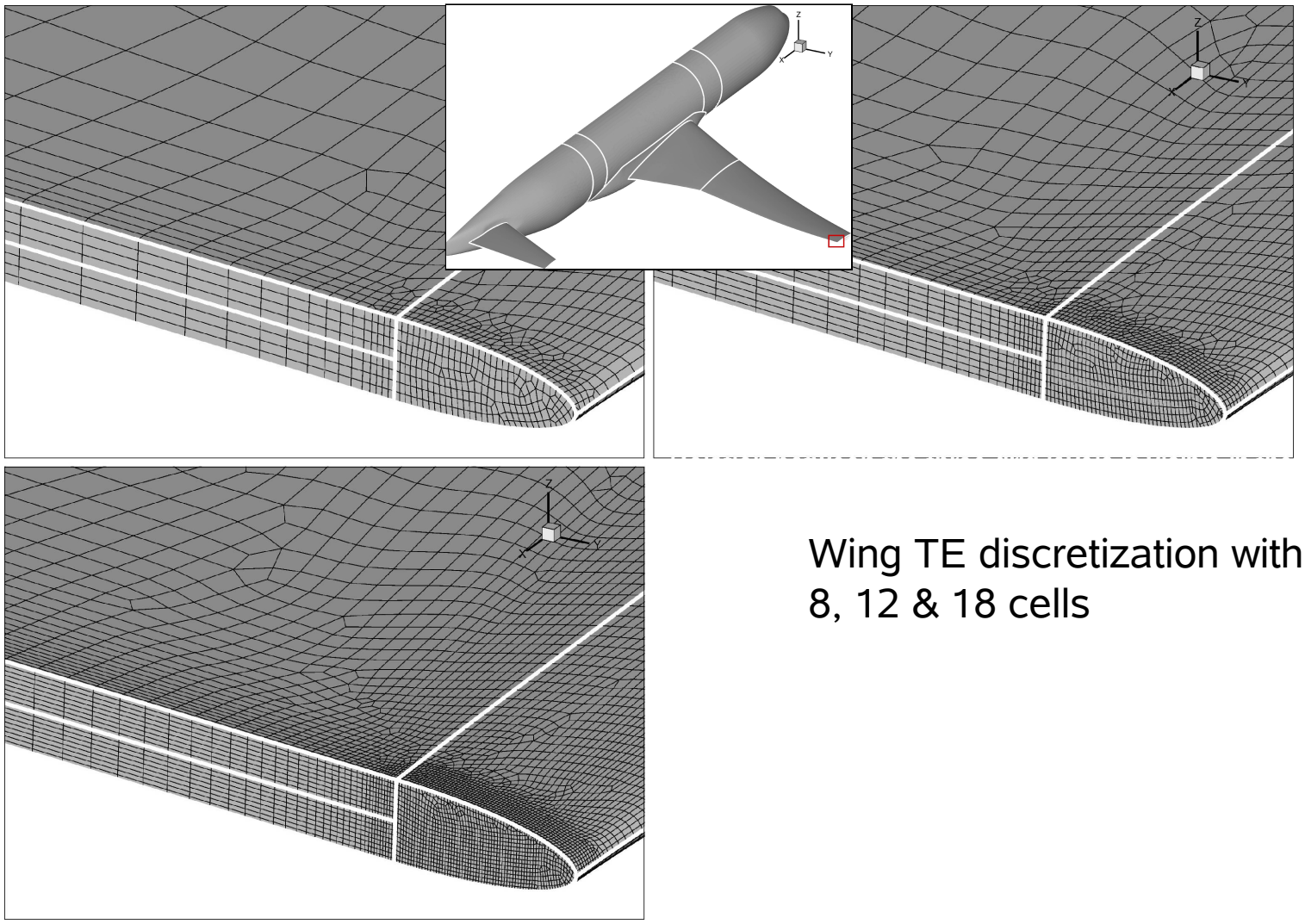

Wing TE discretization with
8, 12 & 18 cells

Grid Family

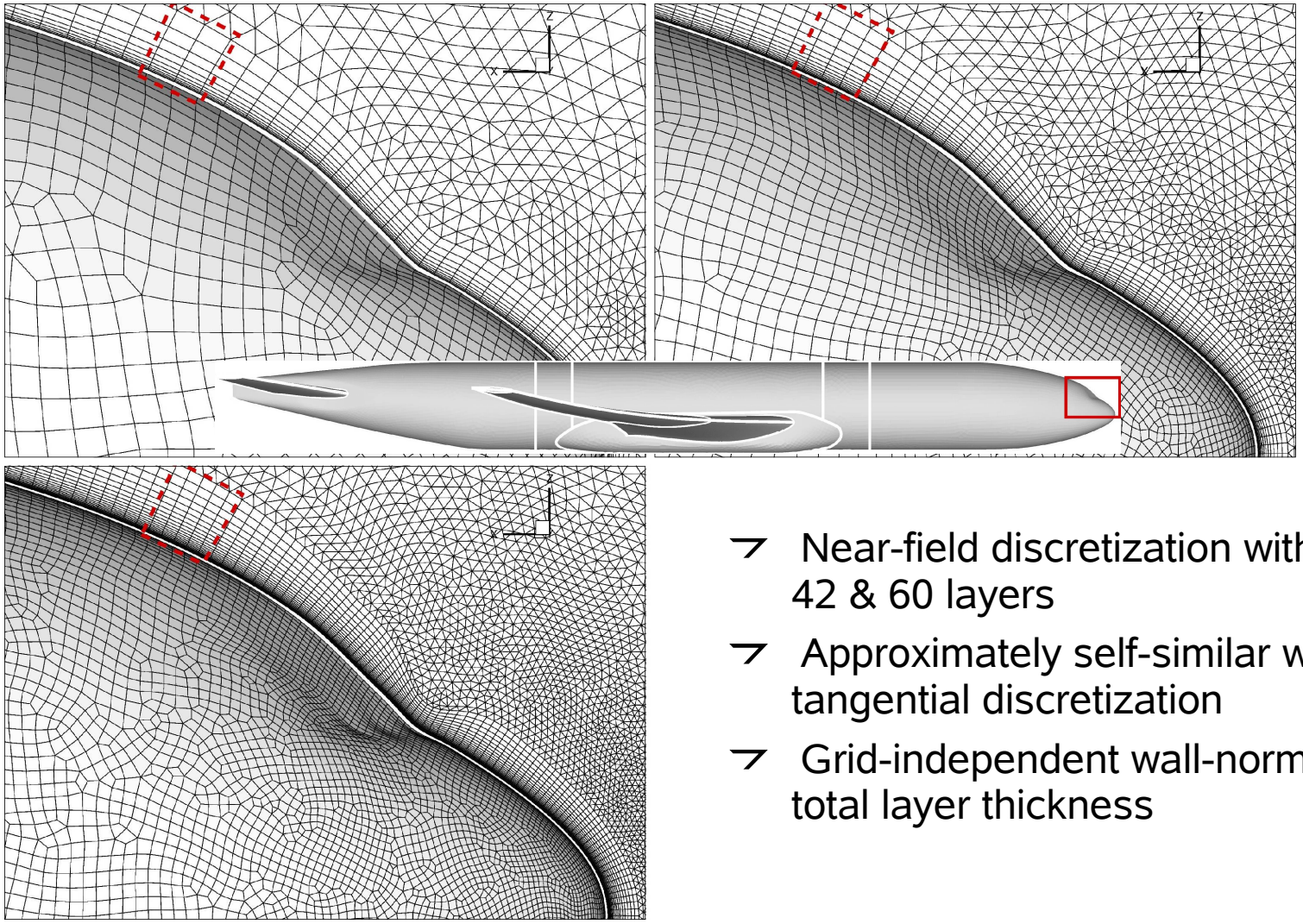

- Near-field discretization with 30, 42 & 60 layers
- Approximately self-similar wall-tangential discretization
- Grid-independent wall-normal total layer thickness

Adjoint-based Grid Improvements

- Identification of regions with high influence of artificial dissipation on specific cost function (C-drag/C-my)
  - Variable 4 (V4) used here as sensor from TAU adjoint solver
- Manual, interactive modification and addition of Solar sources

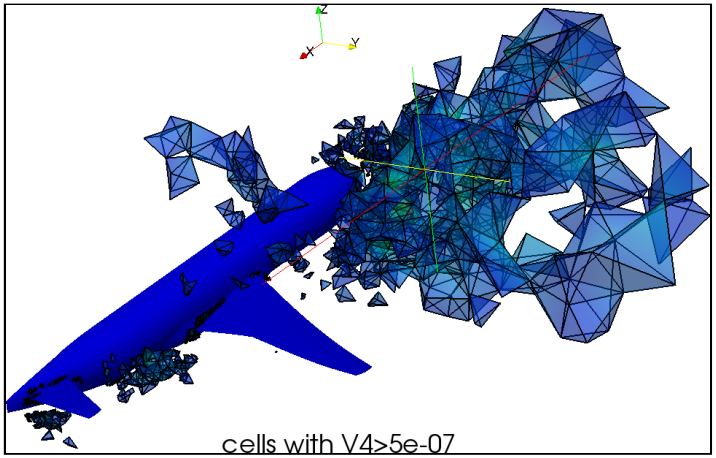

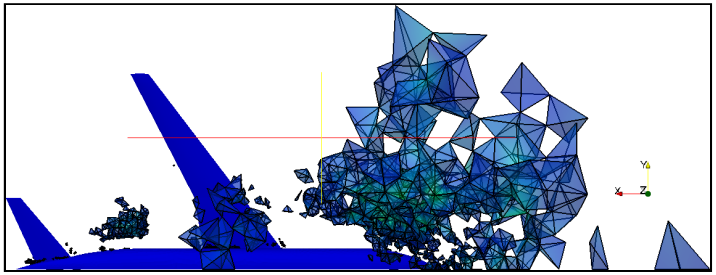

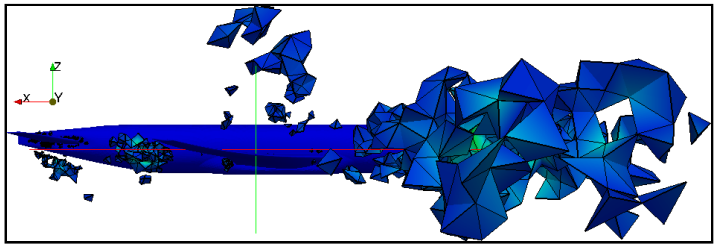

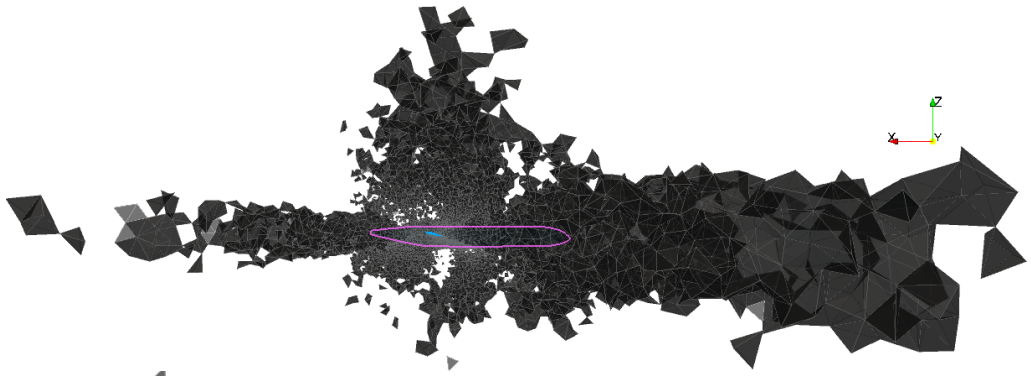

Adjoint-based Grid Improvements

- Identified problematic regions with remedy
  - Fuselage: spacing x0.5
  - Wing- and HTP-fuselage junction: reduce chord-wise anisotropy, increase spacing x1.5
  - Inner wing wake: spacing x0.5
  - HTP wake: spacing x0.75
  - Upstream of wing: extend upstream wing tri-sources; spacing x8, r_1x2, r_2x2
  - Wingtip vortex: add wingtip tri-source

Adjoint-based Grid Improvements

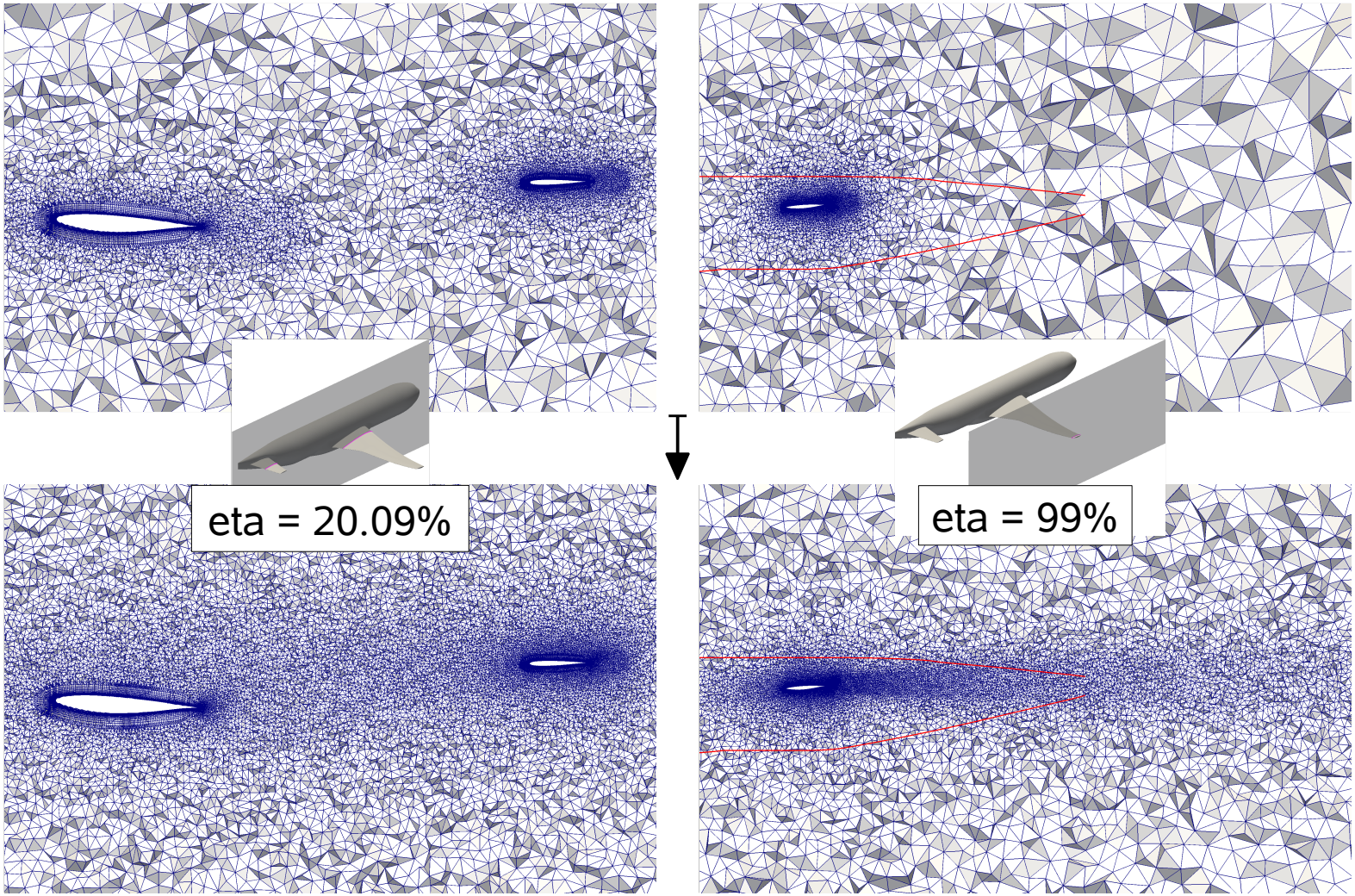

Adjoint-based Grid Improvements

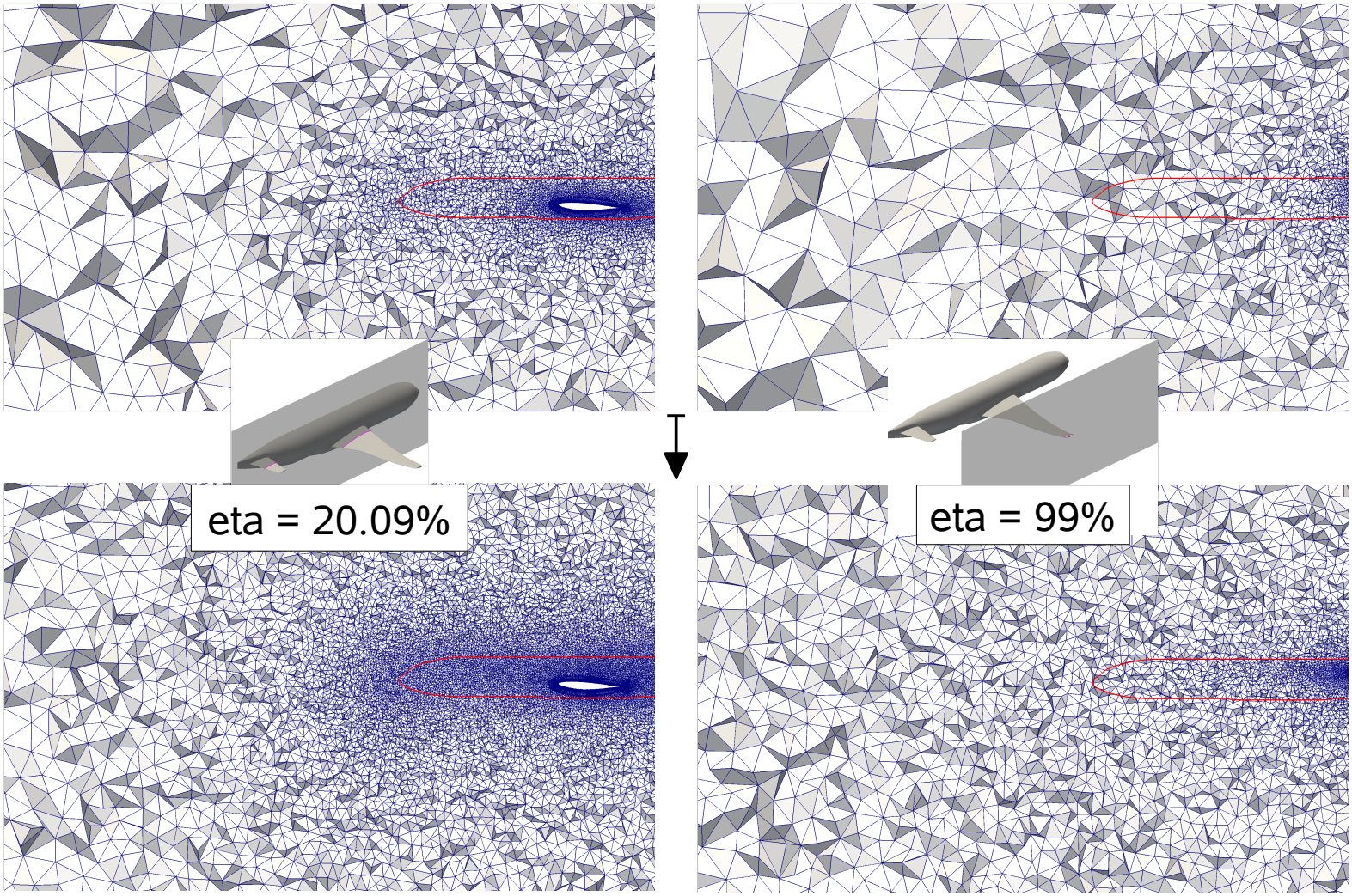

Workshop Summary

- Workshop summary and comparison between all delivered datasets; Solar/TAU: T, C, S (SST, SA, RSM)
- Asymptotic grid convergence
- SST and SA TAU results within scatter of all (SST and SA) structured results

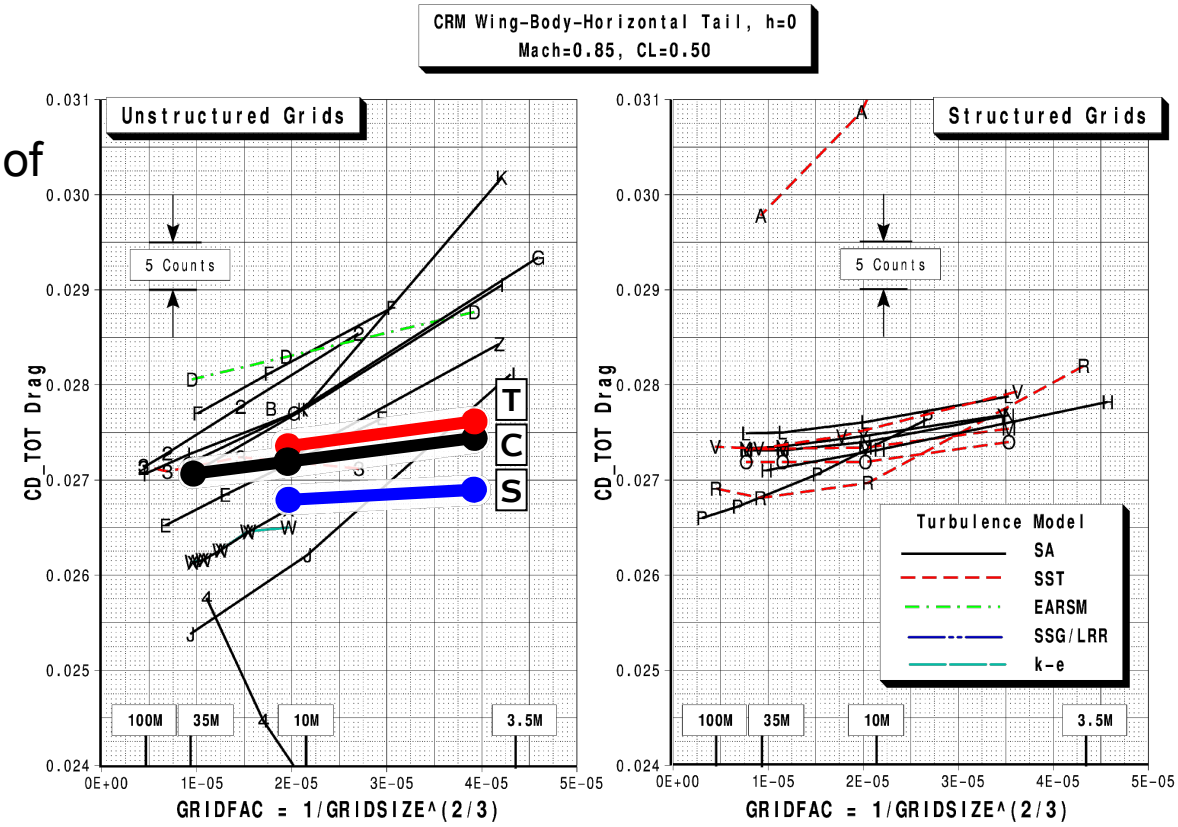

image courtesy: Tinoco et al.

Post-Workshop Activities

- Wing-body separation bubble at trailing edge
  - Some participants predict one, others don't
  - Solar/TAU (all grids, all turbulence models) no separation

No reported separation

ID	Turb. Model
C	SA
D	EARSM
L	SA
M	SST k-w
N	SA
O	SST k-w
S	SSG/LRR
T	SST

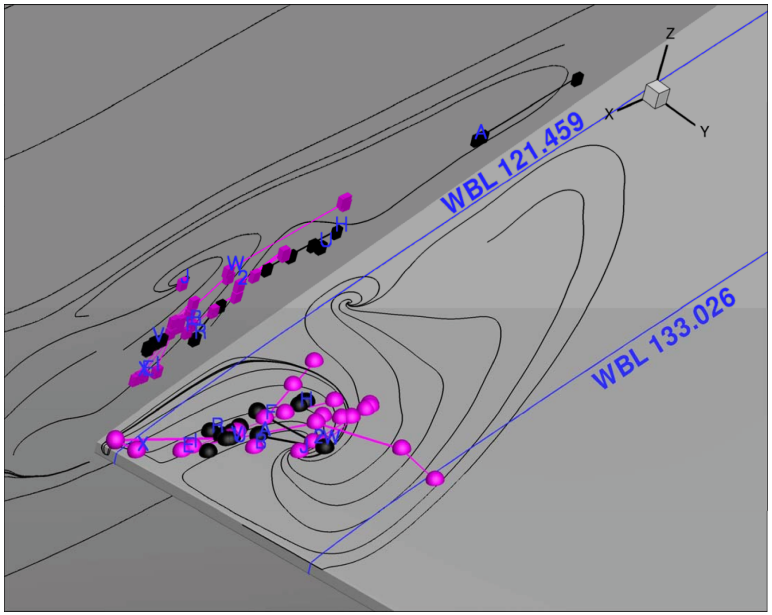

Reported Separation

ID	Turb. Model
A	SST k-w
B	SA
E	SA
F	SA
H	SA
I	SA
J	SA
P	SA
R	SST k-w
U	SA
V	SST k-w
W	k-e
X	SA
2	SA
4	SA

image courtesy: Tinoco et al.

Post-Workshop Activities

- Hints of insufficient wing-body junction discretization observed from the adjoint solution

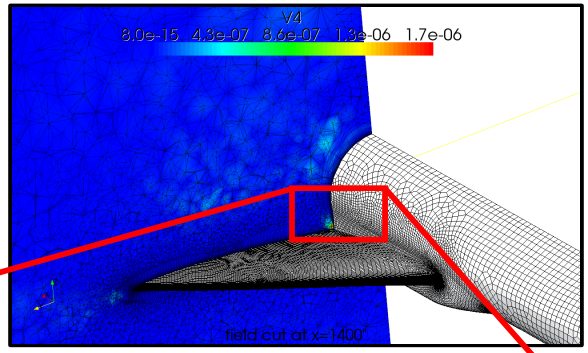

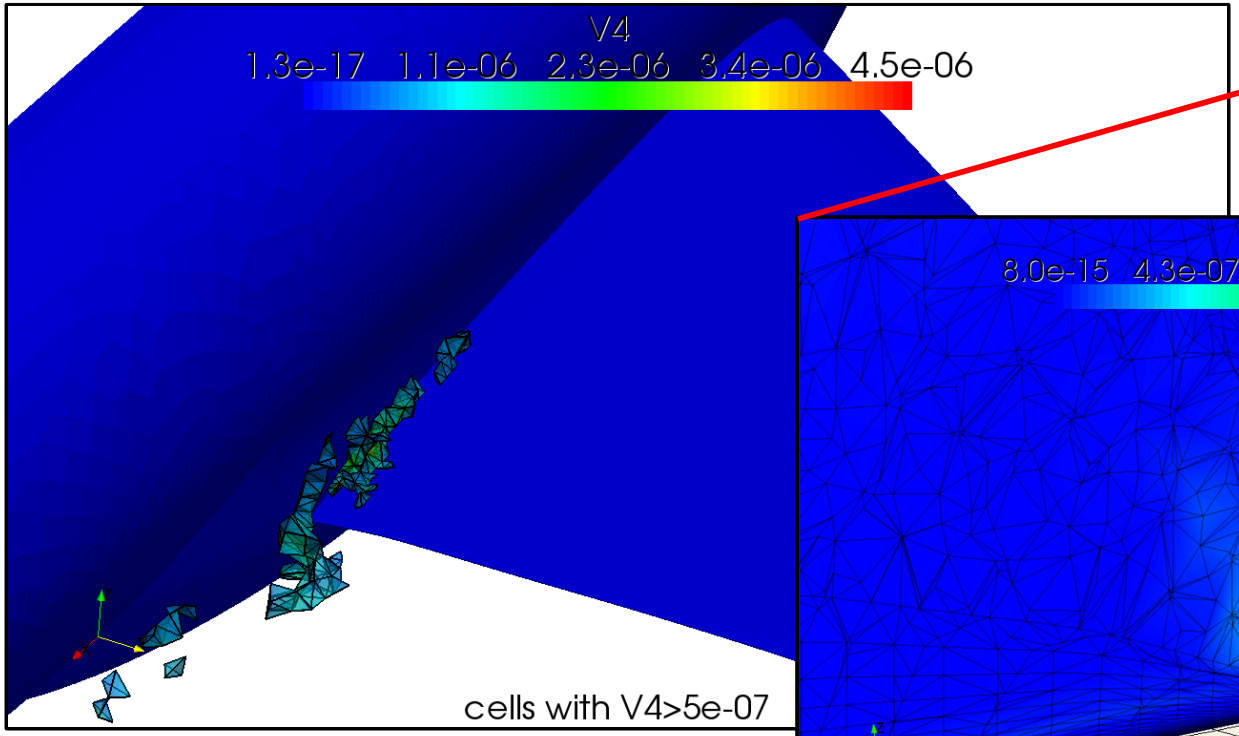

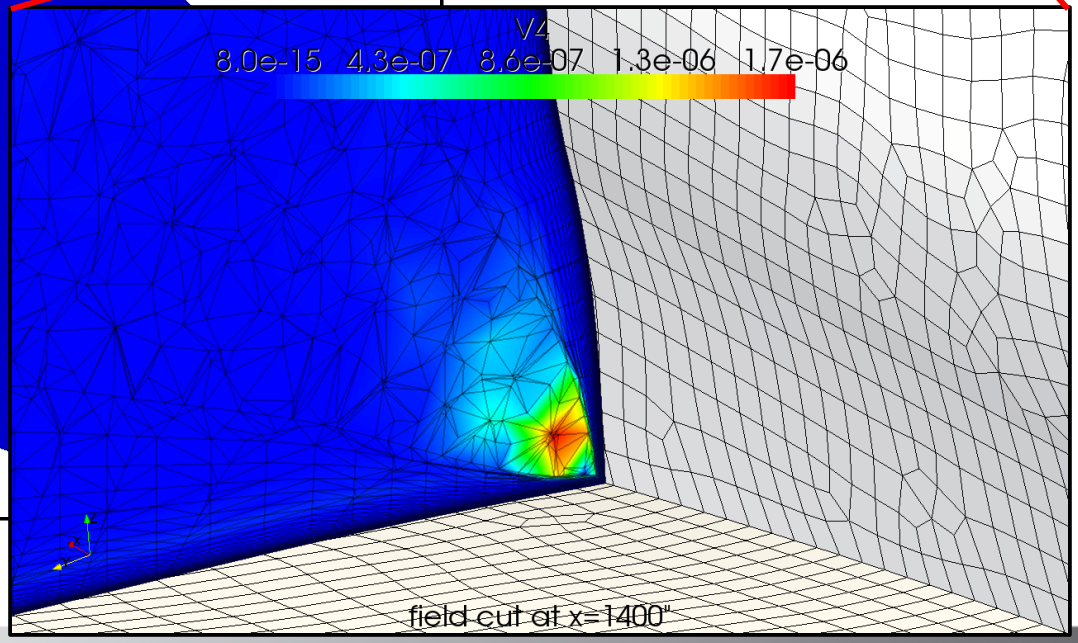

Post-Workshop Activities

- Solver-side solution approach to junction near-field contraction via overset grid (chimera)
- C-H (C/90°) block initially constrained to wing/body TE region

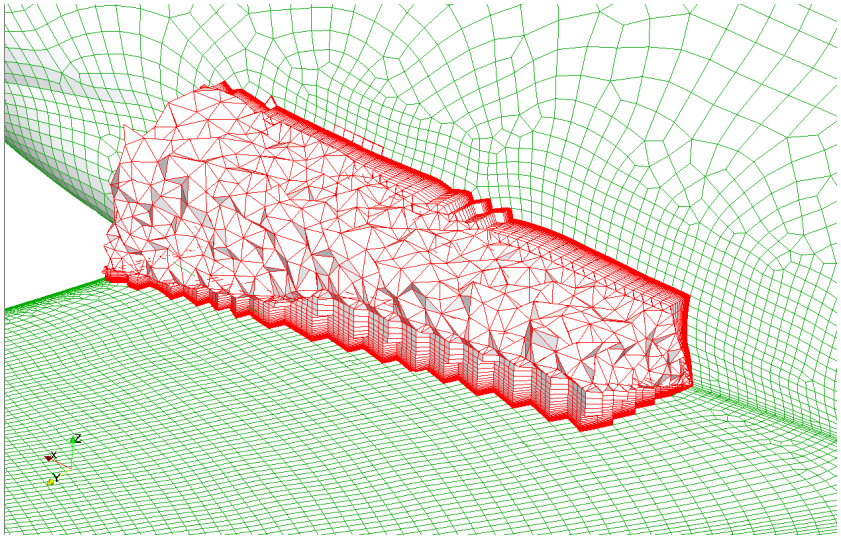

Cut-out from Solar grid

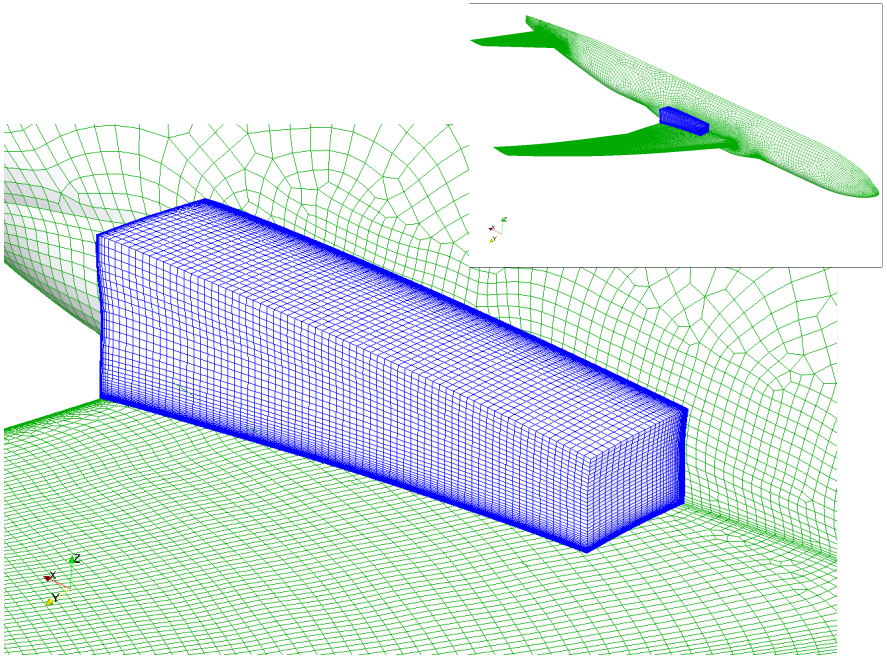

New computational domain

Post-Workshop Activities

- Based on study of resulting BL profiles from initial hexa block, switch to complete C-H block around entire wing root and wake
  - Same first cell height and expansion ratio at overlap
  - Chimera grid composed of Solar medium grid (11.7 mio. points) + hexa (5.5 mio. Points)

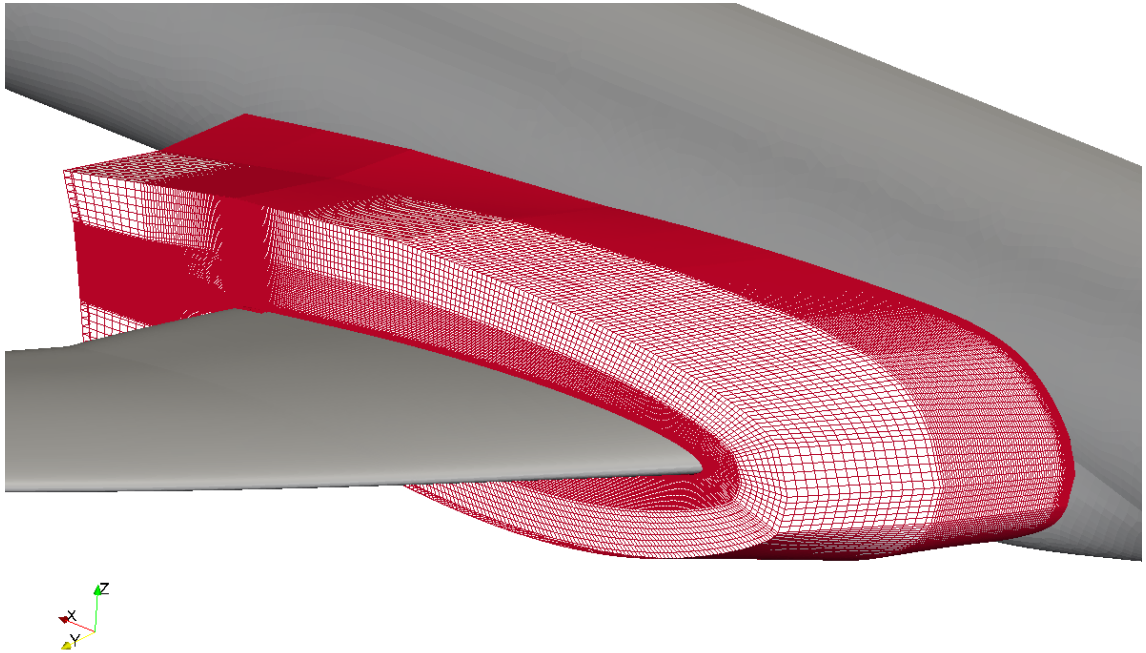

Post-Workshop Activities

- Orientation for the following slides
  - View from the rear to the front, rotated by 10° around the z-axis

Clean wall surfaces

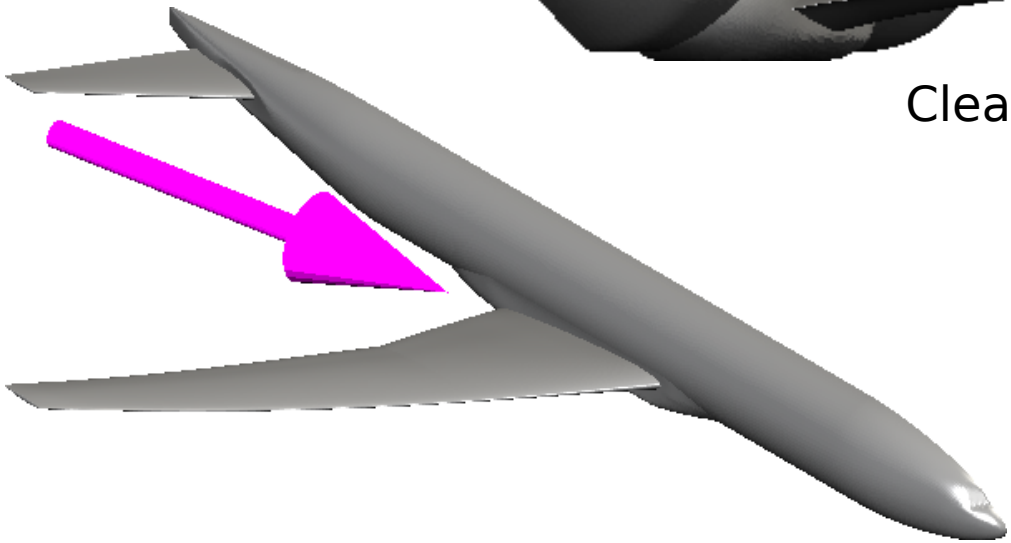

View direction on TE of wing-body junction

Post-Workshop Activities

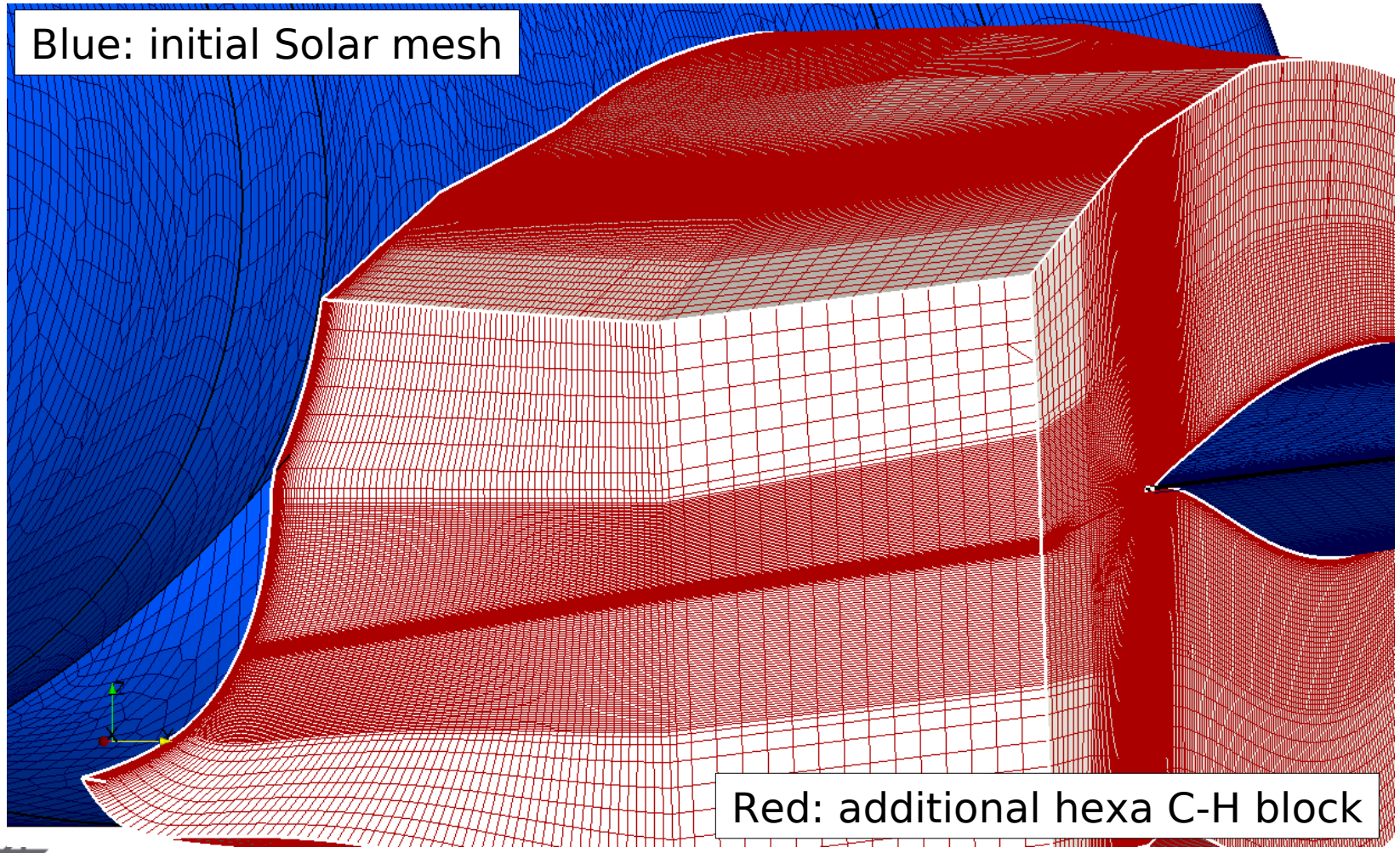

Post-Workshop Activities

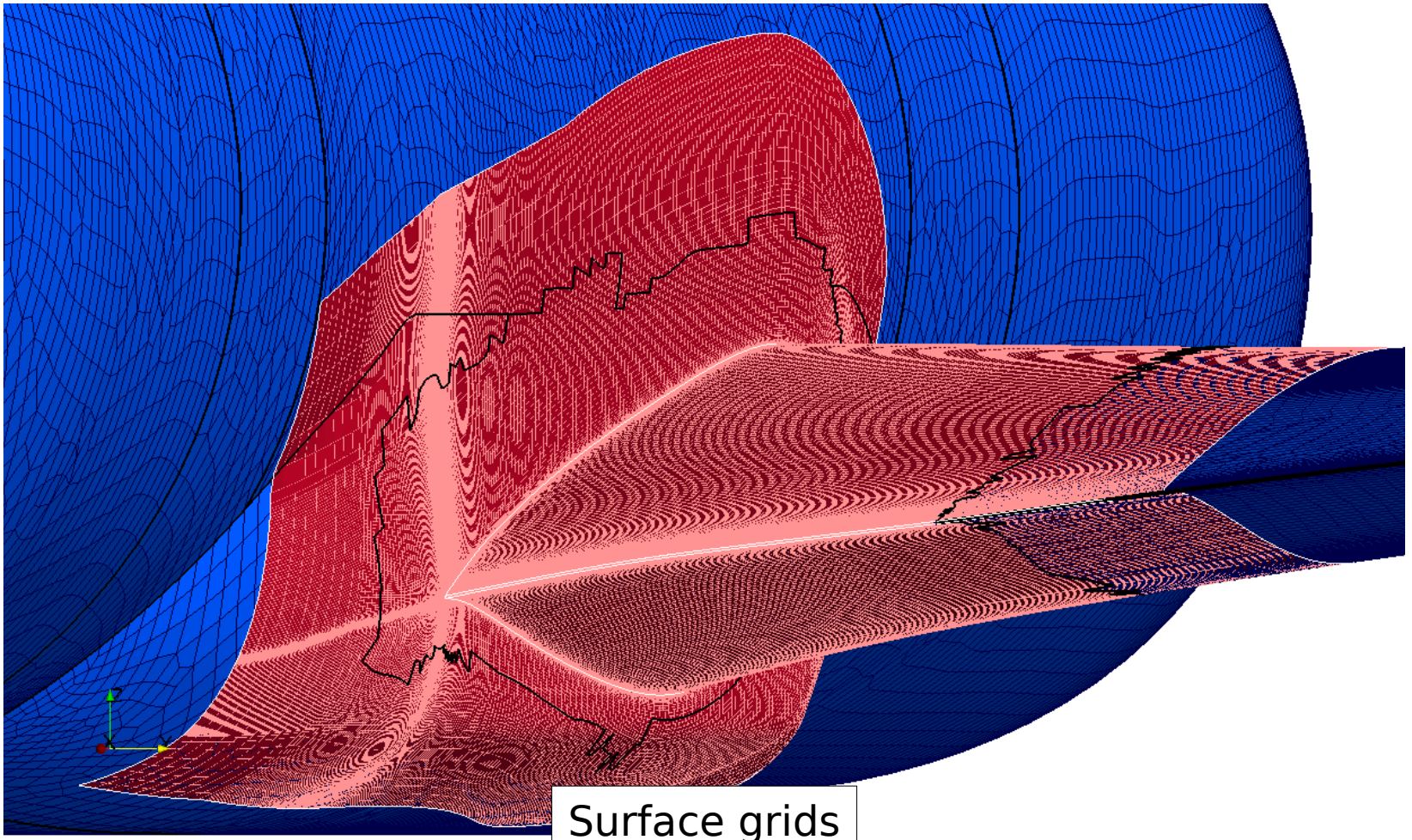

Post-Workshop Activities

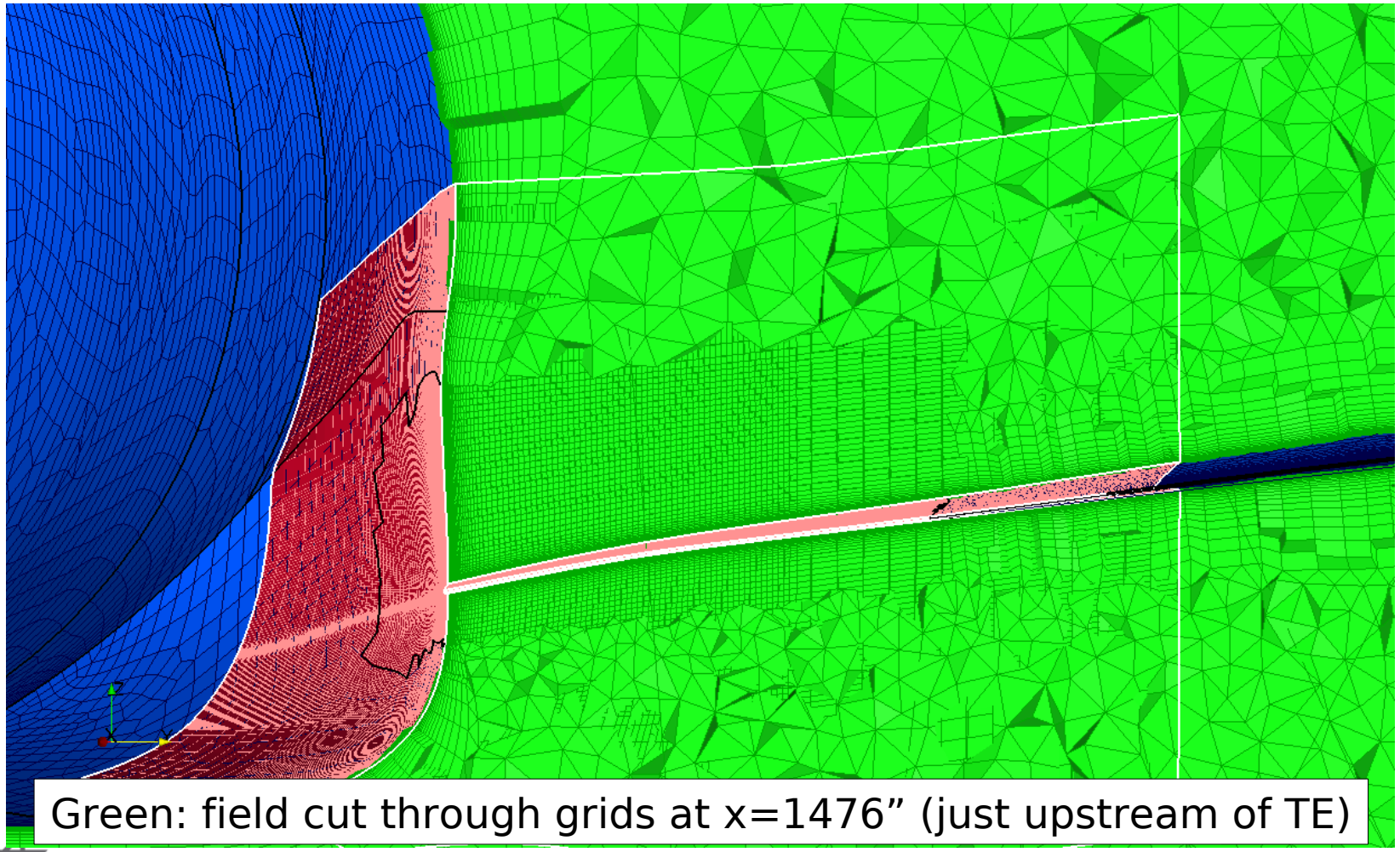

Green: field cut through grids at x=1476” (just upstream of TE)

Post-Workshop Activities

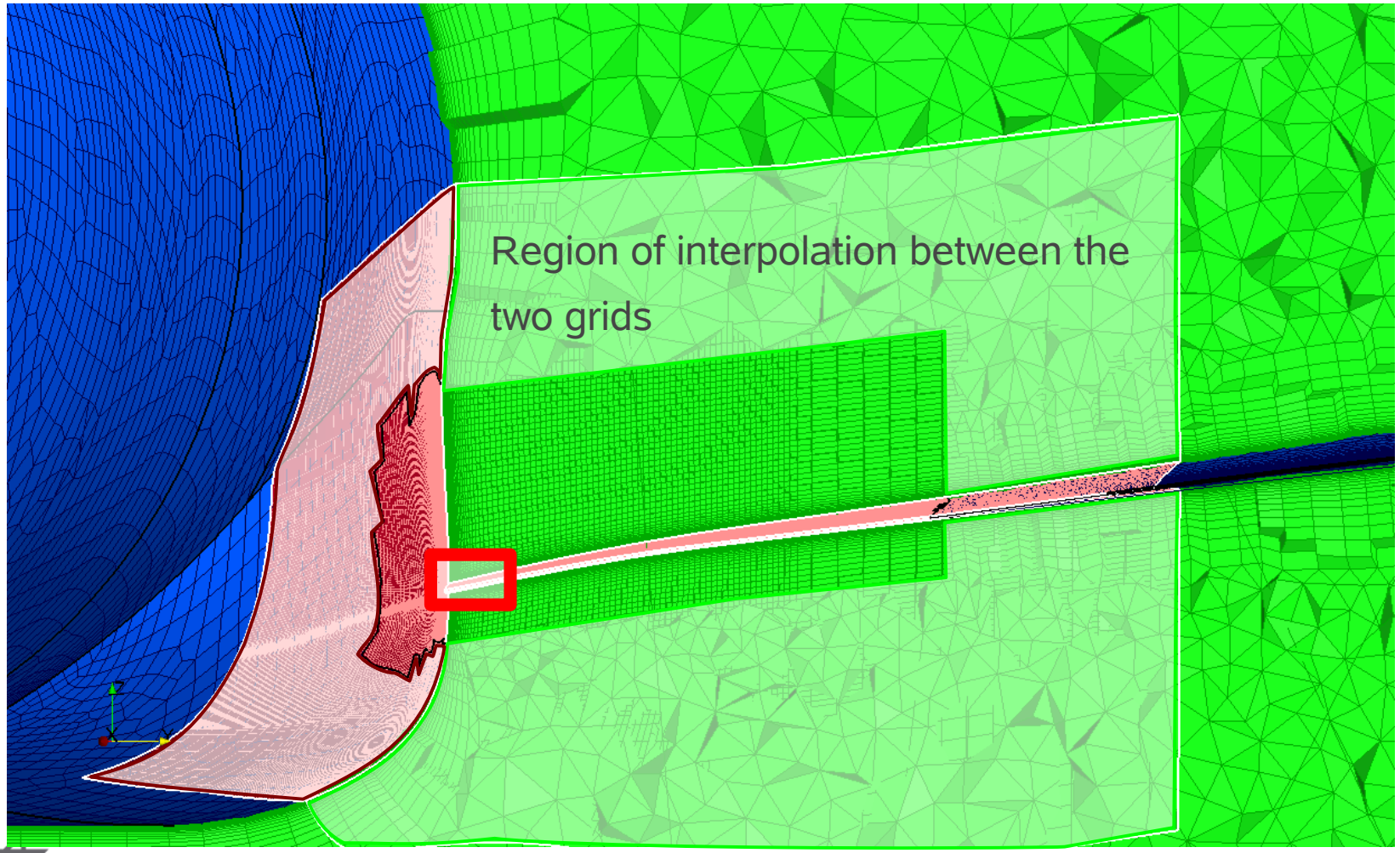

Post-Workshop Activities

- Comparison between original Solar grid and hexa block of chimera grid, reveals the improved field discretization directly above the near-field layers

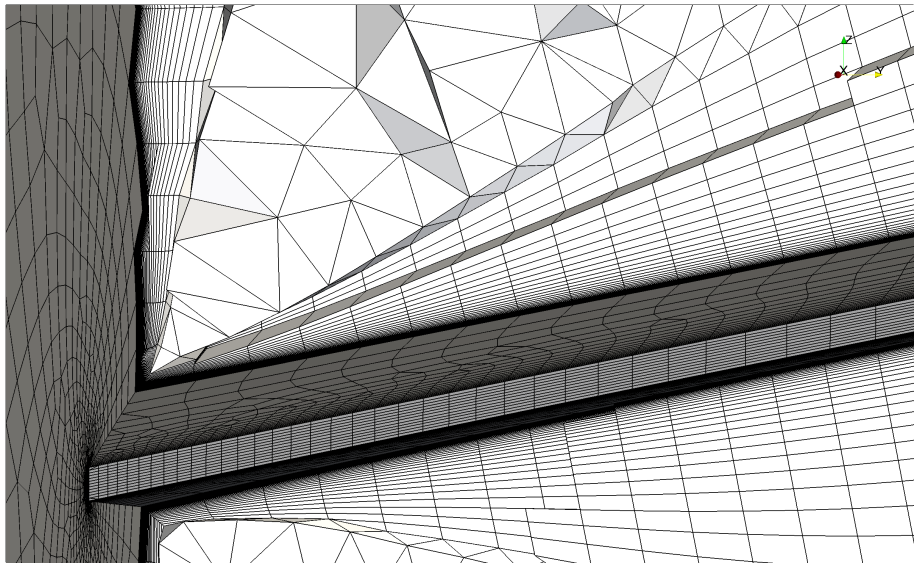

Original Solar grid

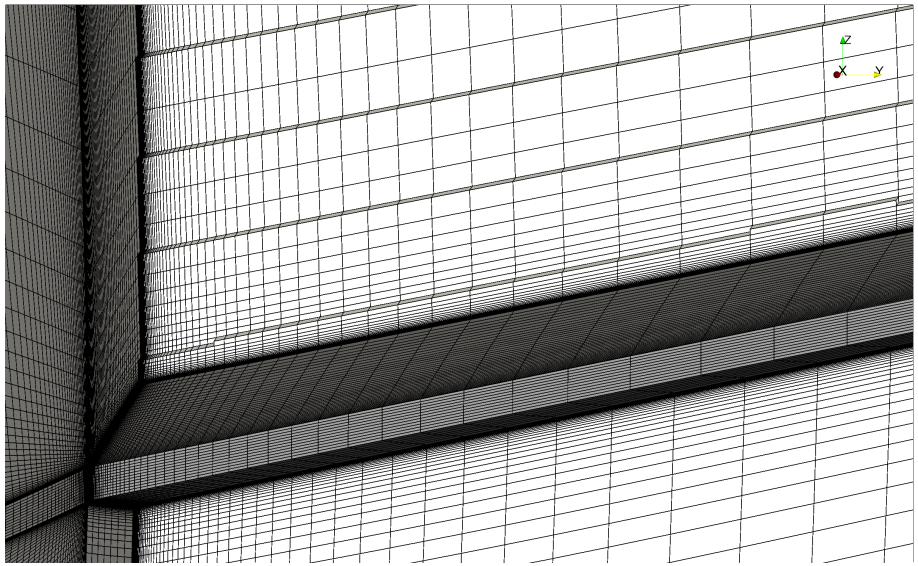

Hexa block of chimera grid

Post-Workshop Activities

- Solar & hexa chimera grid is relatively fine, when compared to other (medium) structured grids

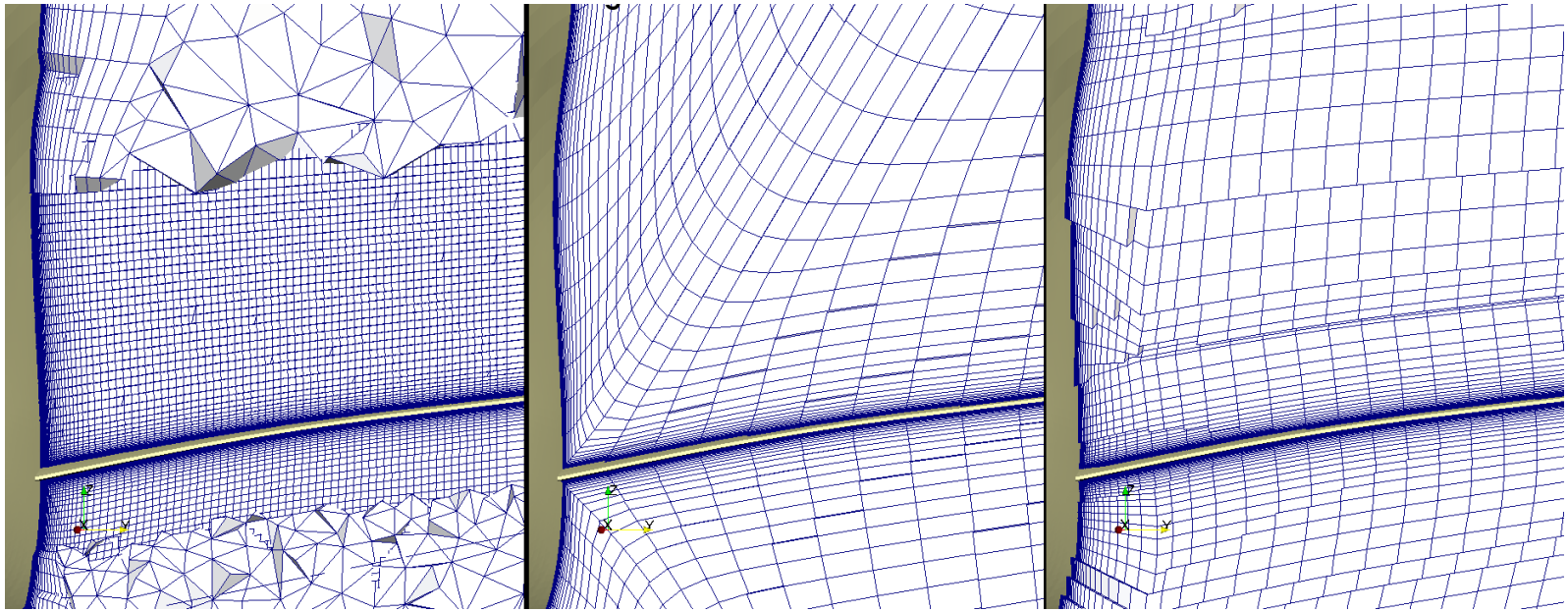

Solar & hexa block grid Boeing ANSYS

Post-Workshop Activities

- Through improved field discretization, the separation bubble is resolved for target-C-lift = 0.5 computations (case 1.1; aoa ≈ 2.3°)

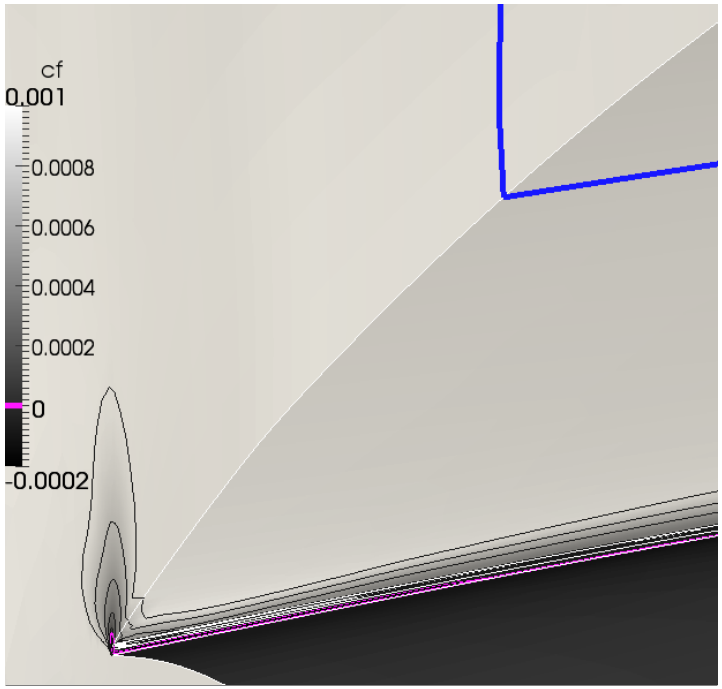

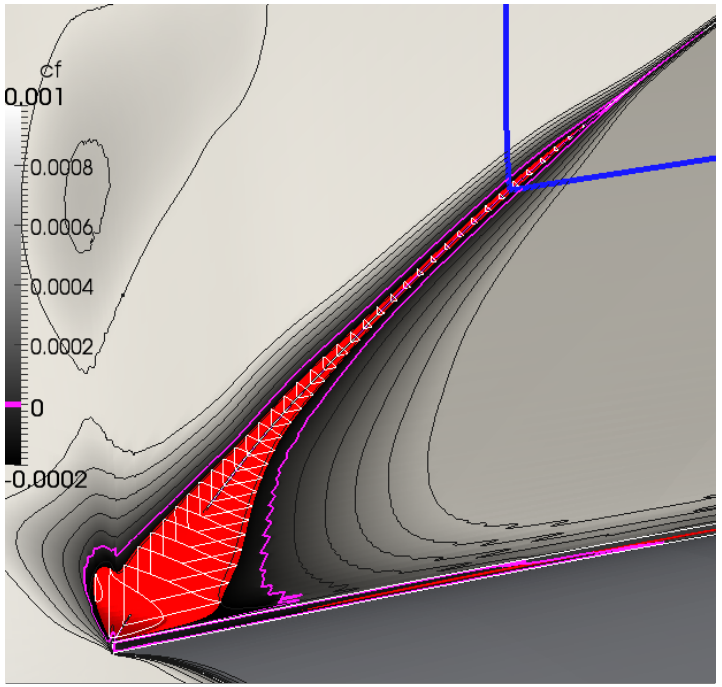

- Solution on original Solar grid (left) reveals the same location of the shock (isocurve of critical pressure coefficient in blue) as on the chimera grid (right)
- Separation bubble (isosurface of x-velocity = -10 m/s in red) starts ahead of sonic line

Post-Workshop Activities

- Surface pressure and skin friction data compared at the innermost cut-plane of y/2b=10.5%
- First experimental cut-plane at y/2b=13.06% outside of influence region of separation bubble

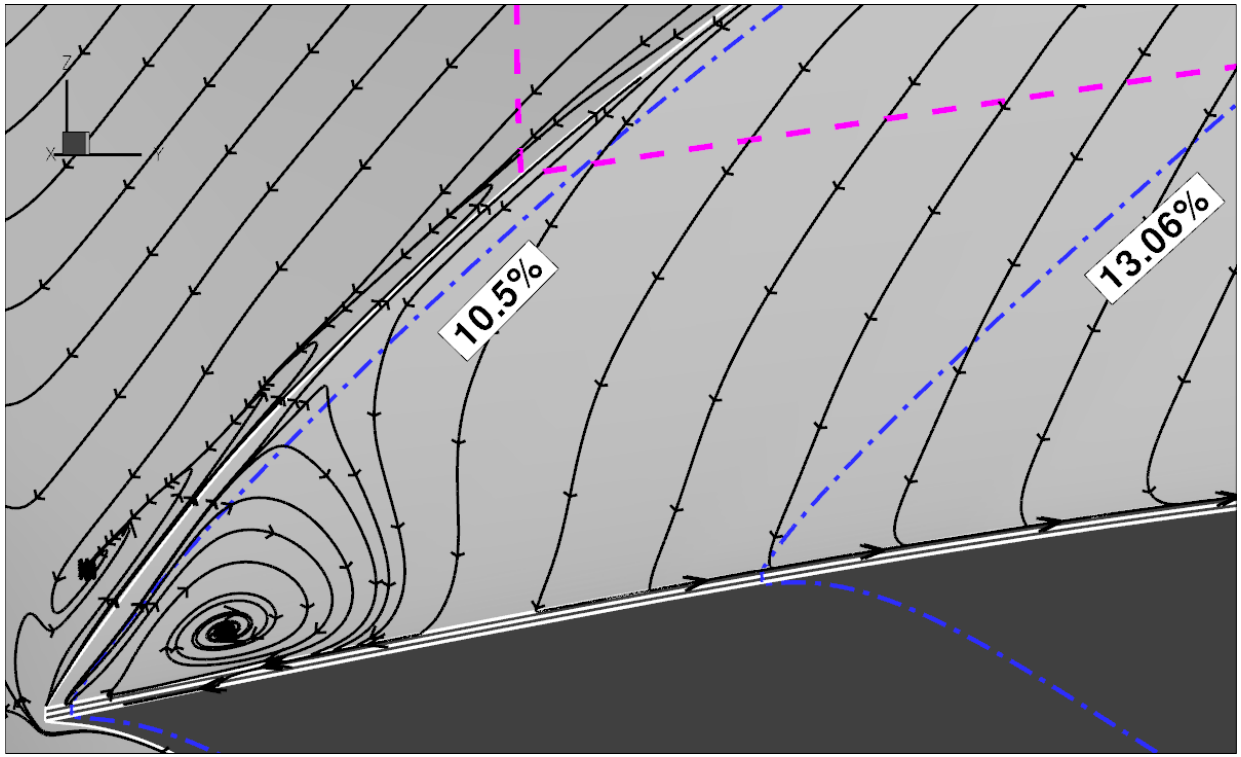

Post-Workshop Activities

- No difference in pressure rise over shock between the two solutions
- Separation visible (only) through skin friction coefficient

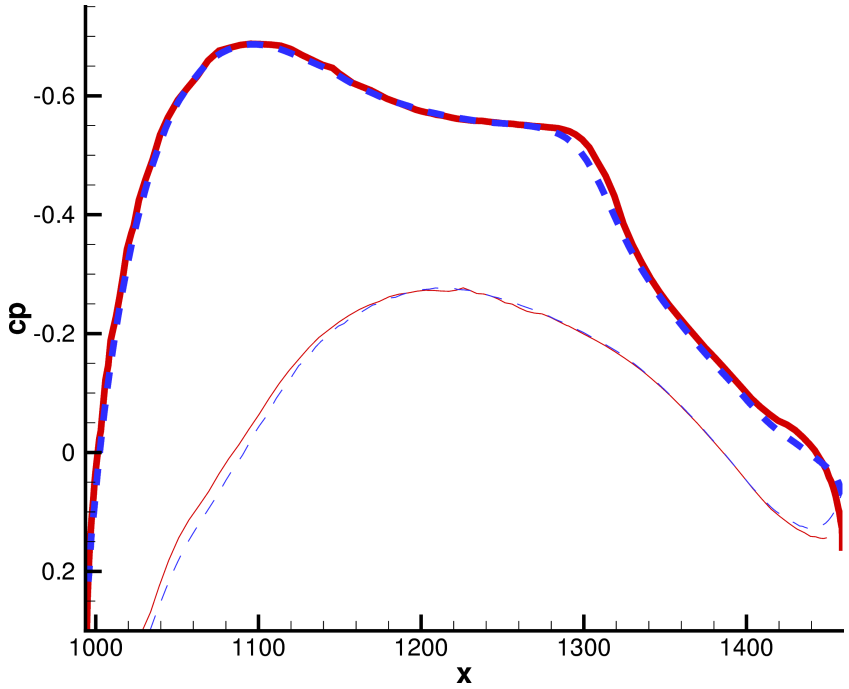

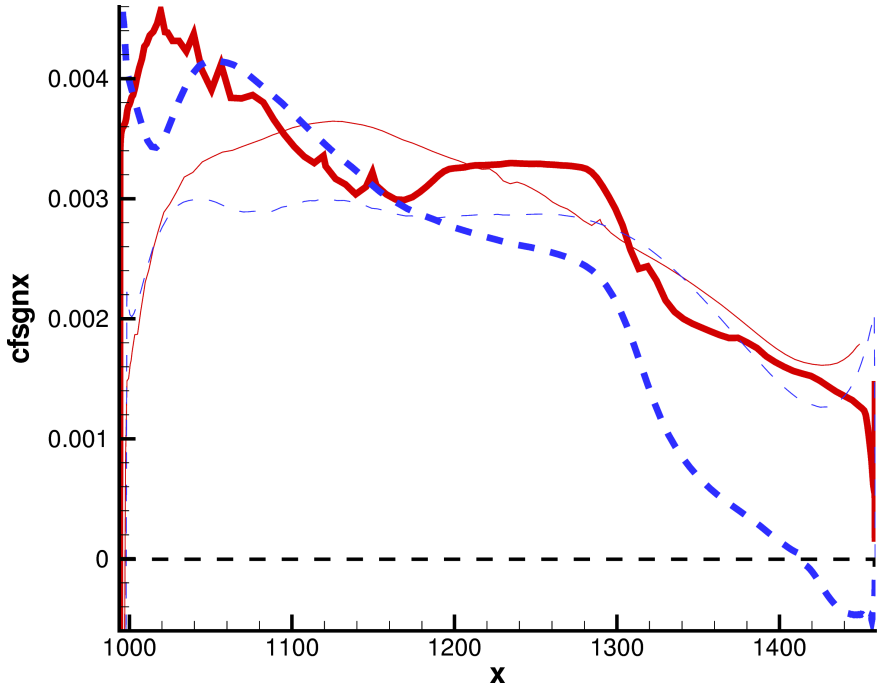

Case 1.1; Solar grid (red, continuous) compared to chimera grid solution (blue, dashed) at y/2b=10.5%; pressure coefficient (left) and skin friction coefficient (right) for SA computations; upper wing data bold

Post-Workshop Activities

- No separation found with other turbulence models on Solar grid (SA, SST, RSM)

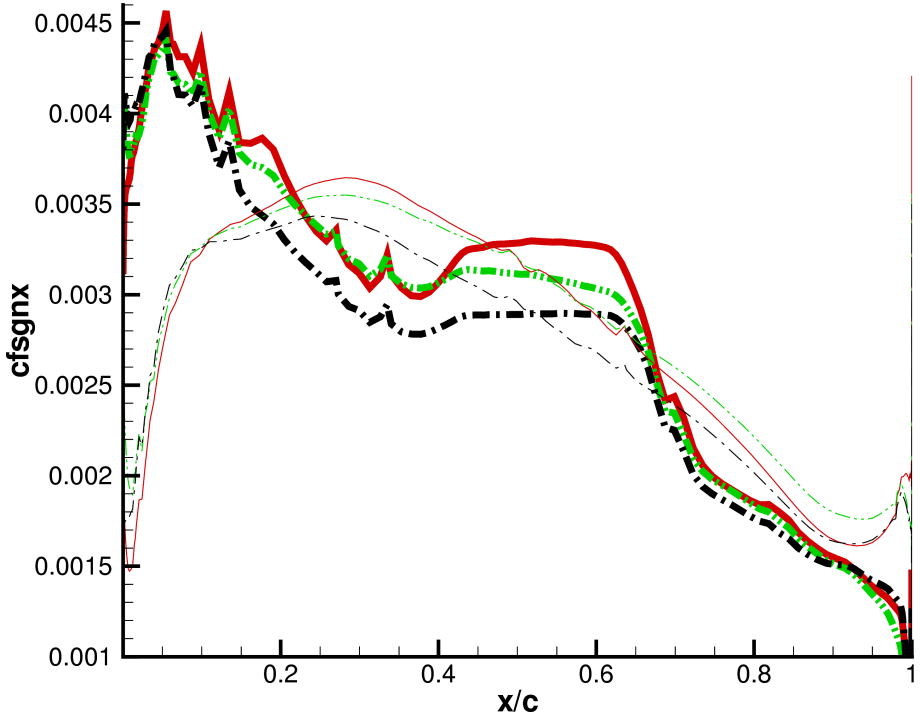

Case 1.1; Solar grid, SA (red, continuous), SST (green, dash-dot-dot) and RSM (black dash-dot) results at y/2b=10.5%; skin friction coefficient; upper wing data bold

Post-Workshop Activities

- On chimera grid, separation is found for all tested turbulence models (SA, SARC, RSM)
- No influence on separation of rotational corrections for SA; RSM topologically similar, but separation is bigger

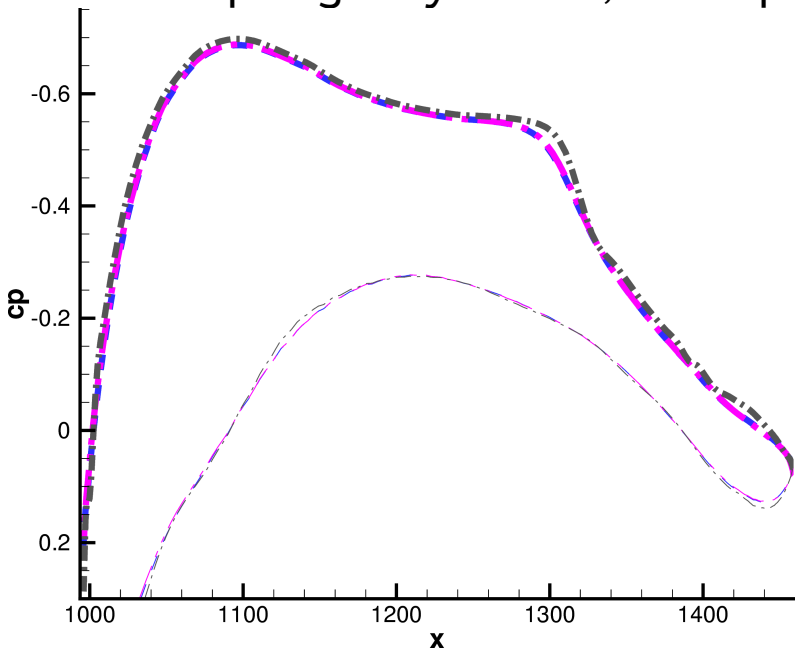

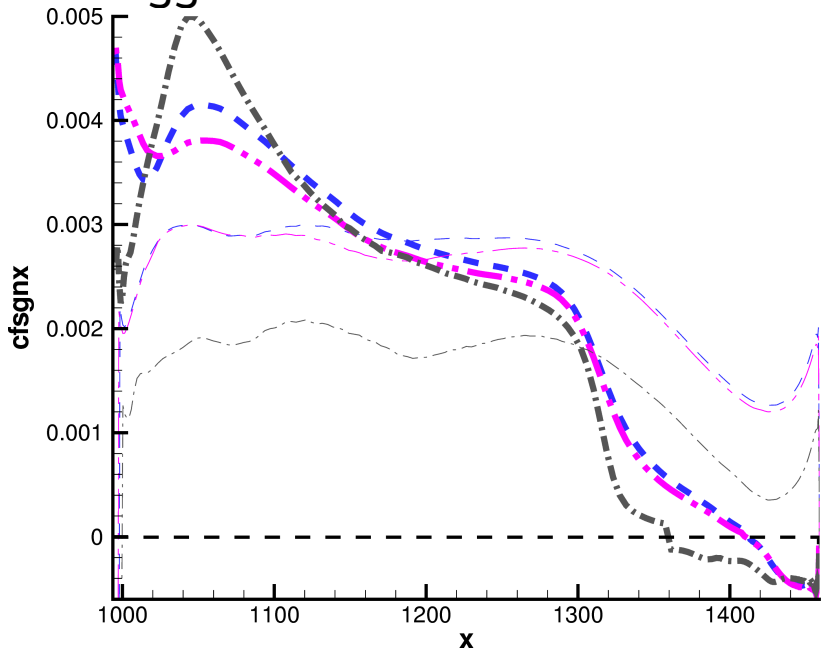

Case 1.1; Chimera grid solution for SA (blue, dashed), SARC (pink, dash-dot-dot) and RSM (gray, dash-dot) at y/2b=10.5%; pressure coefficient (left) and skin friction coefficient (right); upper wing data bold

Post-Workshop Activities

- At the edge of the envelope (aoa = 4°), the inferior junction discretization of the standard Solar grid has (more) severe effects
- Begin of separation moves upstream

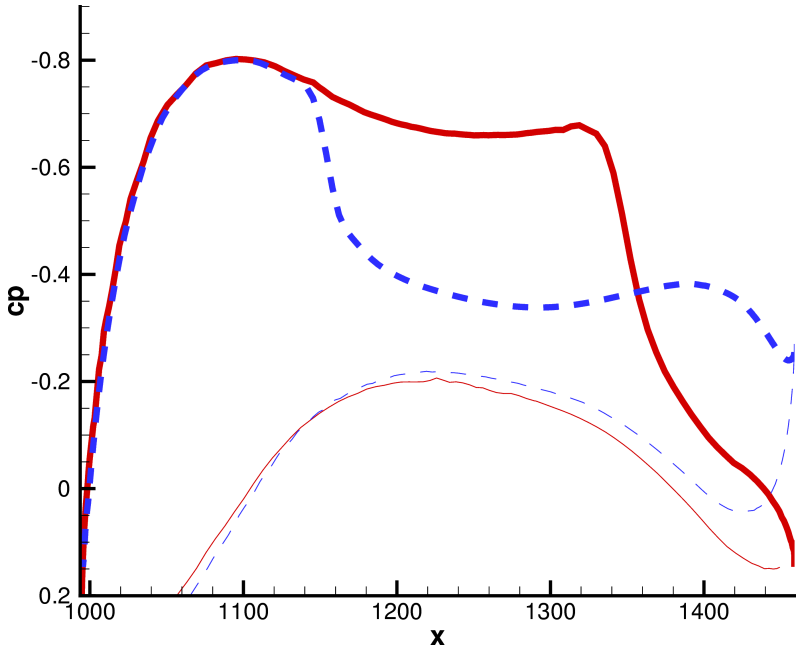

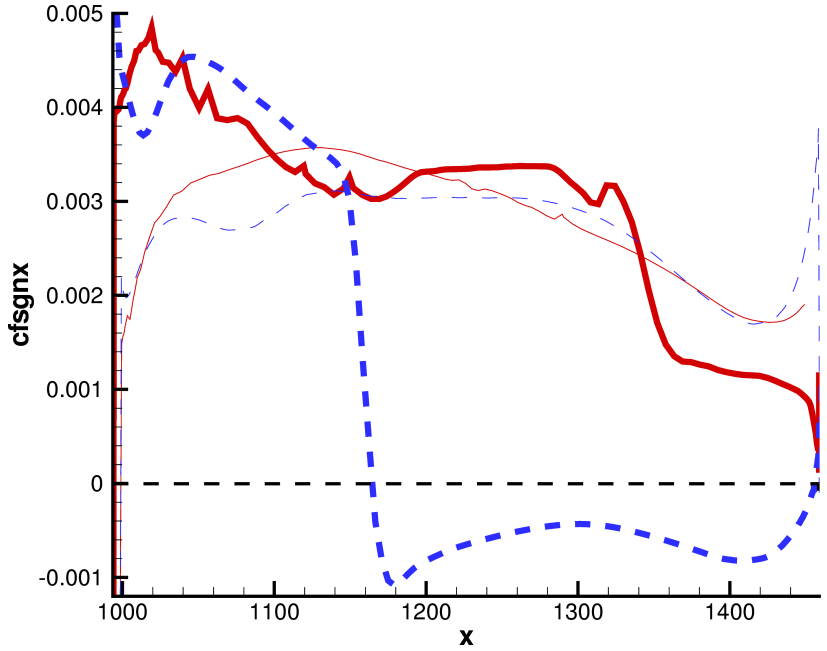

Case 1.2, aoa =4°; Solar grid (red, continuous) compared to chimera grid solution (blue, dashed) at y/2b=10.5%; pressure coefficient (left) and skin friction coefficient (right); upper wing data bold

Post-Workshop Activities

- Massive separation bubble dominates inner wing flowfield in chimera grid solution

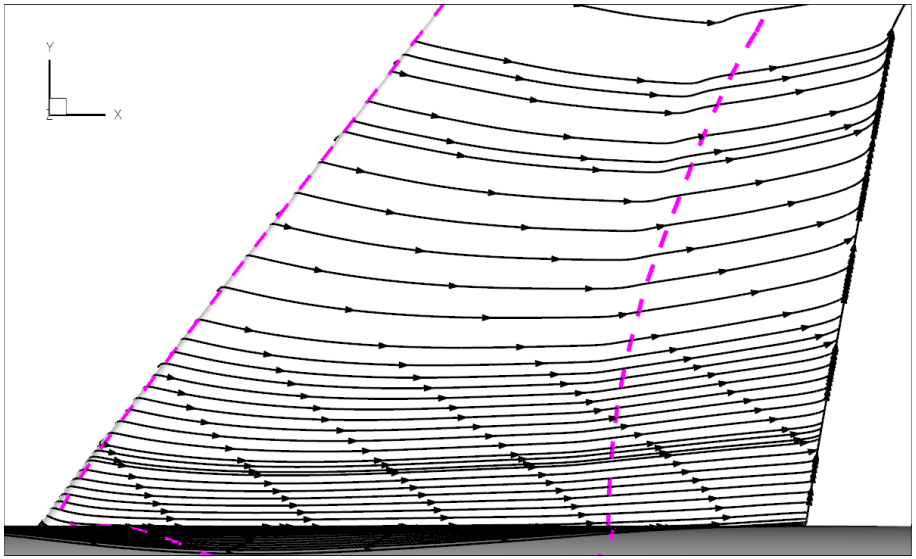

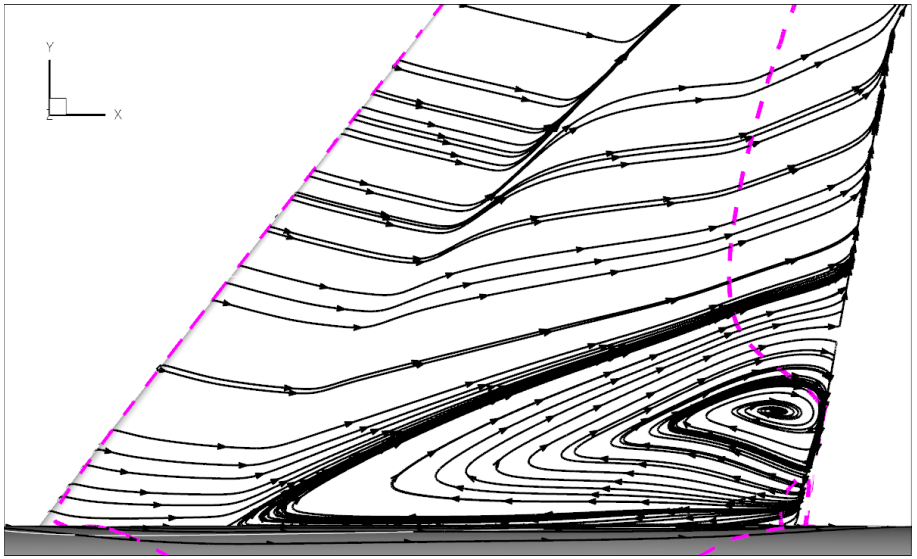

Case 1.2, aoa =4°; Solar grid (left) compared to chimera grid solution (right); critical pressure coefficient (pink, dashed curve) and skin friction lines

Conclusions

- Grid family generation process developed for Solar, applicable to any advancing-layer/front method
  - Satisfactory grid convergence; behavior (second order) and gradient
  - Even without resolution of separation bubble at SOB (not resolved on any grid level)
- Performed successful adjoint-based grid assessment and improvement
- Grid deficiency for junction flow discretization solved via chimera grid technique
  - At Cl=0.5, separation onset seemingly triggered by shock destabilizing effect on junction boundary layer
  - At aoa=4°, substantial change in wing root flow topology